

Wednesday Evening, August 5, 2026

International Workshop on Gallium Oxide and Related Materials (IWGO-6)

Room Concourse - Session IWGO-WeP

IWGO Poster Session III

Moderators: Hari Nair, Cornell University, Saurav Roy, North Carolina State University

IWGO-WeP-1 Ultra-Sensitive Arc-Detecting DUV Sensor based on p-NiO/ β -Ga₂O₃ Heterojunction Using p⁺ NiO Interlayer, Taejun Park, Yusup Jung, Sanghun Kim, TaiYoung Kang, SinSu Kyoung, Powercubesemi, Inc., Republic of Korea

Ultraviolet (UV) radiation from the sun can be divided into UV-A (320–400 nm), UV-B (280–320 nm), and UV-C (200–280 nm). Among them, UV-C light is strongly absorbed by the ozone layer at the earth's surface, so it is also called solar-blind deep UV light (DUV). The need for DUV sensing is increased because of its properties such as arc discharge detection in power plants and sterilization. And DUV sensor research has been extensively conducted in various fields, including biological and chemical analyses, arc detectors, and flame sensors [1].

In this study, we simply fabricated a DUV sensor based on p-NiO/ β -Ga₂O₃ heterojunction by the RF sputtering system. In addition, the experiment was conducted to investigate the effect of p⁺NiO interlayer on the electrical and photoresponse characteristics of the as-fabricated DUV sensor.

As a result, the as-fabricated DUV sensor with p⁺ NiO interlayer had a low leakage current of 7.34×10^{-9} A, high photocurrent of 4.01×10^{-6} A, fast rise and fall times of 30 and 50 ms were observed under UV-C irradiation at -5V bias. The effect of p⁺NiO interlayer on p-NiO/ β -Ga₂O₃ heterojunction DUV sensor has confirmed their potential for application in DUV and Arc detecting systems, and further research is planned to improve the device characteristics.

IWGO-WeP-2 Electrical Characterization of Mist-CVD HfO_x/ β -Ga₂O₃ MIS Capacitor, Hayato Tanikawa, Kyoto Institute of Technology, Japan; Kazutaka Kanegae, Hiroyuki Nishinaka, Kyoto Institute of Technology, Japan
 β -Ga₂O₃ is expected to be used in power switching devices. HfO_x films are one of promising gate dielectrics for β -Ga₂O₃-based devices due to its high dielectric constant. Previous studies have reported HfO_x films deposited by ALD. In this study, mist-CVD was used to deposit HfO_x gate dielectrics. Mist-CVD achieves a deposition rate that is an order of magnitude higher than ALD and does not require vacuum equipment, making it a low-cost technique.

A 40-nm-thick HfO_x film was deposited on HVPE β -Ga₂O₃ epitaxial layers by mist-CVD using the solution gas of O₂, with an O₂/O₃ gas mixture as the carrier gas. The deposition temperature was set to 400°C. The dielectric constant of the mist-CVD HfO_x film was 10.8. Post-deposition annealing (PDA) was performed at 350°C for 10 min in N₂ ambient. Finally, Ni gate and Ohmic electrodes were formed on the HfO_x surface and backside of the β -Ga₂O₃ epitaxial wafer, respectively.

Capacitance-voltage (C-V) characteristics of MIS capacitor were measured at 1MHz. The voltage sweeps were set from -3 V to 7 V (1st sweep) and from 7 V to -3 V (2nd sweep). The experimental C-V curves have a positive voltage shift relative to the ideal curve. Using the flat-band voltage shift of 2.70 V, we extracted a net negative fixed charge density of $Q_f = 6 \times 10^{-7}$ C/cm², which is comparable to the values for ALD HfO_x (10^{-7} to 10^{-6} C/cm²). Hysteresis was observed in the measured C-V characteristics. From the flat-band voltage hysteresis of 0.8 V, we estimated an averaged interface trap density of $D_{it,ave} = 2 \times 10^{11}$ cm⁻² eV⁻¹, which is also comparable to the values for ALD HfO_x (10^{10} to 10^{12} cm⁻² eV⁻¹). With the addition of PDA treatment, Q_f and $D_{it,ave}$ decreased to 4.6×10^{-7} C/cm² and 1.3×10^{11} cm⁻² eV⁻¹, respectively.

In the HfO_x/ β -Ga₂O₃ MIS structure, we successfully formed a HfO_x film by mist-CVD at a higher deposition rate than ALD, with Q_f and $D_{it,ave}$ comparable to those of ALD HfO_x. HfO_x deposited by mist-CVD is a promising gate dielectric for β -Ga₂O₃ power switching devices.

IWGO-WeP-3 Tuning the Conductivity of p-type Ni_{1-x}O Thin Films for Ni_{1-x}O/ β -Ga₂O₃ Heterojunction Power Devices, Thomas Ribault, Akash Patnaik, Bruno Berini, Corinne Sartel, CNRS-UVSQ, France; Yunlin Zheng, Jean-Louis Cantin, CNRS-INSP, France; Zurab Kushitashvili, Amiran Bibilashvili, Institute of Nano et Microelectronics, Tbilisi, Georgia; Tom Micottis, Farid Medjdoub, CNRS-I.E.M.N., France; Ekaterine Chikoidze, Yves Dumont, CNRS-UVSQ, France

Several research groups in the past, reported NiO/ β -Ga₂O₃ rectifiers performance through empirical optimisation of device structure and edge termination [1-4]. However, a well-established materials-physics framework

for sputtered Ni_{1-x}O thin films remains missing. Present work fills this gap by establishing how reactive RF sputtering deposition at room-temperature controls the structural, chemical, and point defect landscape of Ni_{1-x}O, and which in turn governs Ni_{1-x}O/ β -Ga₂O₃ heterojunction structure band alignment, interface quality, carrier transport, and breakdown capability.

Ni_{1-x}O thin films were deposited using reactive RF magnetron sputtering by varying the O₂ fraction from 0 to 100%, and the applied RF power from 50 to 200 Watts. 20-200 nm thin films were deposited primarily on c-sapphire (0001). The room-temperature resistivity decreases, from 5 Ω .cm (50 W) to 0.9 Ω .cm (200 W), and from 30 Ω .cm (20% O₂) to 0.01 Ω .cm (100% O₂), with ~1nm RMS roughness (AFM). XRD patterns consistently show a cubic NiO (111) phase, and the best crystalline quality obtained between 40-60% O₂. NIR transmittance decreases with increasing O₂ fraction, since Ni vacancy and hole carrier density increases, which enhances free-carrier absorption. Kelvin probe measurements show that the work function of Ni_{1-x}O remains constant at 4.23 eV for films deposited at 20-90% O₂, which implies constant Fermi level, thus, indicating hopping conductivity mechanism with localised carriers. The optimised Ni_{1-x}O thin films with different thicknesses were then deposited on 10 μ m Si: β -Ga₂O₃ (001) epilayers from NCT, Japan. Subsequently, vertical Ni_{1-x}O/ β -Ga₂O₃ heterojunction PiN diodes were fabricated, which exhibits rectifying behaviour with a V_{ON} ~1.9 V and low leakage current densities ~10⁻⁷-10⁻⁸ A/cm². Thus, this study will enable to engineer p-type Ni_{1-x}O film using room-temperature RF sputtering technique, for the realization of high-breakdown voltage β -Ga₂O₃ heterojunction power devices.

References

- [1] S. J. Pearton *et al.*, *A.P.R.*, 5, 011301 (2018)
- [2] J.-S. Li *et al.*, *A.P.L.*, 121, 042105 (2022)
- [3] H. Gong *et al.*, *IEEE*, 67, 8, 3341-3347 (2020)
- [4] A. Taube *et al.*, *M.S.S.P.*, 184, 108842 (2024)

IWGO-WeP-4 Electro-Optical Metrology Development to Probe Deep-Level Traps in β -Ga₂O₃ MOSFETs, Ory Maimon, George Mason University; Neil Moser, Air Force Research Laboratory; Pragya Shrestha, Min-Yeong Kim, National Institute for Science and Technology (NIST); Sang-Mo Koo, Kwangwon University, Republic of Korea; Kyle Liddy, Andrew Green, Kelson Chabak, Air Force Research Laboratory; Qiliang Li, George Mason University; Sujitra Pookpanratana, National Institute for Science and Technology (NIST)

Although the performance of β -Ga₂O₃ high power devices as field-effect transistors (FETs) have progressed rapidly in recent years, device performance is hindered by defects and traps. Traditional trap characterization methods are sensitive to shallow traps. High densities of traps can significantly reduce mobility by scattering free carriers. However, the long emission time of deep traps in WBG semiconductors requires the use of optical excitation and novel techniques such as deep-level optical spectroscopy, persistent photo-capacitance, photo-assisted C-V (PCV), and photo-assisted I-V (PIV).

In this work, PCV and PIV with sub-bandgap photon energies, E_{hv}, is used to study the ionized impurity scattering of deep level traps in a lateral depletion-mode β -Ga₂O₃ FET. The density of interface trap states (D_{it}) in β -Ga₂O₃ FETs was determined between 0.4 eV – 4.4 eV below the conduction band (EC) of β -Ga₂O₃. D_{it} peaks near the band edges, similar to conventional material systems. Based on the results, traps located between EC – 4.0 eV and EC – 3.4 eV are primarily responsible for carrier scattering, reducing the mobility by 50 % – 75 % in these devices. The increased mobility degradation further from the interface is attributed to traps located in the bulk.

Author for correspondence: sujitra@nist.gov

IWGO-WeP-5 The Morphology of the Cr₂O₃ Films Surfaces Analyzed by Multifractal Formalism, Pavel Butenko, Ioffe Institute, Russian Federation
It is a completely new state-of-art work that analyses diverse surface morphologies of the Cr₂O₃ films deposited on sapphire substrates by mist CVD via Multifractal formalism.

In this abstract, we characterize the surface relief using Multifractal formalism, which determines a number of geometric features that allow us to evaluate various parameters of multifractality. The conditions under which the film shows the maximum nonlinear complexity of the surface, which is required for its functionality, are found. Contrary to the roughness assessment and the regular fractal approach, the multifractal formalism is able to perform in-depth surface morphology analysis necessary to verify the effectiveness of the surface. This will be useful for various functional

applications, for example, the sensor capability of Cr_2O_3 , which is a promising wide bandgap semiconductor material.

IWGO-WeP-6 Growth of 2-inch n-type $\beta\text{-Ga}_2\text{O}_3$ (011) Single Crystal by the VB Method, Yuki Ueda, Takuya Igarashi, Kimiyoshi Koshi, Sho Hasegawa, Ryoichi Sakaguchi, Taiki Chujo, Ryo Shinagawa, Kohei Sasaki, Akito Kuramata, Novel Crystal Technology, Inc., Japan

Homoeptaxial growth of $\beta\text{-Ga}_2\text{O}_3$ on (011) substrates using the halide vapor phase epitaxy (HVPE) method has attracted attention because it enables high-purity films to be formed that have very flat surfaces. However, the conventional edge-defined film-fed growth (EFG) method is limited in the crystal orientations that can be grown, making large-diameter (011) substrates difficult to obtain. In this study, we attempted to grow a 2-inch $\beta\text{-Ga}_2\text{O}_3$ (011) crystal using the vertical Bridgman (VB) method, which enables a wider variety of crystal orientations to be grown than the EFG method.

(011) seed crystals and sintered Ga_2O_3 raw materials were loaded into a Pt-Rh alloy crucible, and crystal was grown in a resistance-heated VB furnace. The raw material was co-doped with 0.05 at% Sn and 0.005 at% Si. The crystal was grown by lowering the crucible at a rate of 1 mm/h. As a result, we successfully grew a 2-inch n-type $\beta\text{-Ga}_2\text{O}_3$ (011) single crystal using the VB method and fabricated a 2-inch $\beta\text{-Ga}_2\text{O}_3$ (011) substrate. The average full width at half maximum (FWHM) of the x-ray rocking curve (XRC) 022 peak over five points on the substrate was 38 arcsec, indicating high crystallinity. In addition, Hall effect measurements revealed a minimum resistivity of $27 \text{ m}\Omega \cdot \text{cm}$ and showed n-type conductivity.

IWGO-WeP-7 c- In_2O_3 Growth by Oxide Vapor Phase Epitaxy Using In_2O and H_2O Source Gases, Rie Togashi, Takumi Shimazaki, Sophia University, Japan; Masato Ishikawa, Gas-Phase Growth Ltd., Japan

Single-crystalline cubic In_2O_3 (c- In_2O_3) has attracted considerable attention as a wide-bandgap semiconductor material for next-generation optoelectronic devices. For such applications, it is essential to prepare high-quality c- In_2O_3 single-crystal layers with low carrier density and high carrier mobility. In recent years, the growth of single-crystalline c- In_2O_3 layers in the bixbyite phase has been reported using halide vapor phase epitaxy (HVPE) [1]. On the other hand, $\beta\text{-Ga}_2\text{O}_3$ growth using Ga_2O and H_2O source gases has been reported [2]. Based on this oxide-source-gas approach, we investigate c- In_2O_3 growth by oxide vapor phase epitaxy (OVPE) using In_2O and H_2O source gases. In this method, In_2O gas is selectively generated by supplying H_2O vapor over In metal in the source zone. The c- In_2O_3 layer is then formed through the reaction between the generated In_2O gas and additional H_2O vapor in the growth zone. In this study, c- In_2O_3 growth using In_2O and H_2O source gases was investigated through both experiments and thermodynamic analysis.

Thermodynamic analysis was first carried out for the formation of In_2O through the reaction between H_2O gas and In metal in the source zone under atmospheric pressure. The calculated equilibrium partial pressures indicated that In_2O can be generated efficiently at elevated temperatures through the reaction $\text{H}_2\text{O}(\text{g}) + 2\text{In}(\text{l}) = \text{In}_2\text{O}(\text{g}) + \text{H}_2(\text{g})$.

Next, thermodynamic analysis was performed for the formation of c- In_2O_3 through the reaction between In_2O gas and H_2O gas in the growth zone under atmospheric pressure. The driving force for c- In_2O_3 formation was determined from the equilibrium analysis. The results showed that the driving force increased with increasing input partial pressure of In_2O , indicating that the reaction $\text{In}_2\text{O}(\text{g}) + 2\text{H}_2\text{O}(\text{g}) = \text{c-}\text{In}_2\text{O}_3(\text{s}) + 2\text{H}_2(\text{g})$ proceeds in the forward direction.

Based on these considerations, c- In_2O_3 were experimentally grown on (0001) sapphire substrates by OVPE using a home-built horizontal hot-wall quartz glass reactor. The experimentally derived driving forces were in good agreement with the thermodynamic predictions. Under H_2O -rich conditions, however, the experimental result deviated from the theoretical value. This is presumably because, in the present system, the reaction between H_2O and the In metal surface becomes saturated under this condition owing to the limited surface area of the In source. As a result, excess H_2O remains unreacted, and the In_2O supply is limited.

[1] R. Togashi *et al.*, Jpn. J. Appl. Phys., **55**, 1202B3 1-5 (2016). [2] R. Togashi *et al.*, Jpn. J. Appl. Phys. (2026), Accepted.

IWGO-WeP-8 Fabrication and Characterization of (011)-Oriented Substrates by the Vertical Bridgman Method, Dong-Jun Lee, Jinki Kang, AXEL, Republic of Korea

$\beta\text{-Ga}_2\text{O}_3$ has attracted significant attention as a next-generation power semiconductor material due to its ultra-wide bandgap and high critical

electric field. In addition, the availability of melt-grown bulk single crystals makes it a promising candidate for large-area substrate applications. Among various crystallographic orientations, the (011) plane is considered a favorable orientation for vertical power-device structures [1].

However, crystal growth along the (011) direction is more challenging than other orientations due to difficulties in maintaining interface stability and managing thermal stress during growth. Meanwhile, fabrication of (011) substrates from conventionally grown (010) crystals requires off-axis cutting, resulting in an elliptical wafer shape and leading to increased material loss and processing complexity.

In this study, the challenges associated with (011)-oriented $\beta\text{-Ga}_2\text{O}_3$ crystal growth using the vertical Bridgman (VB) method were analyzed, and process strategies to overcome these limitations are proposed. The stability of (011) growth was improved through optimization of key process parameters, including temperature gradient and growth rate.

[1] B. Chen, W. Mu, Y. Liu, P. Wang, X. Ma, J. Zhang, X. Dong, Y. Li, Z. Jia, and X. Tao, CrystEngComm **25**, 2404 (2023).

* Author for correspondence: jinki.kang@gmail.com

IWGO-WeP-9 Characterization of p- Cr_2O_3 /n- Ga_2O_3 Heterojunction Rectifiers, Hannah Masten, Frank Kelly, National Research Council; Chinmoy Nath Saha, Yizheng Liu, University of California at Santa Barbara; Tia Gray, National Research Council; Sriram Krishnamoorthy, University of California at Santa Barbara; Marko Tadjer, Naval Research Laboratory

Recently, sputtered Cr_2O_3 has been demonstrated as an effective, drop-in replacement for sputtered p-NiO which typically exhibits significant instability in electrical conductivity over time [1]. This work reports heterojunction rectifiers of ultra-wide bandgap HVPE (001) $\beta\text{-Ga}_2\text{O}_3$ and novel p-type Cr_2O_3 . Details of Cr_2O_3 deposition were reported in Ref. 1. Prior to Cr_2O_3 deposition, approximately $1 \mu\text{m}$ out of the $10 \mu\text{m}$ thick HVPE Ga_2O_3 epilayer was etched off in BCl_3/Ar plasma (800 W ICP, 5 mT, 20 min etch). The motivation for this plasma etch was to evaluate the potential effect of CMP subsurface damage to rectifier electrical performance. Upon etching, one sample was further annealed in ultra-high vacuum at $700 \text{ }^\circ\text{C}$ for ~ 4 hours to remove plasma etch damage [2]. Thus, three samples were prepared: (1) a control sample (no etch), (2) a BCl_3 -etched sample, and (3) an etched and UHV-annealed sample. Figures 1 and 2 show forward-bias I-V characteristics measured on samples (1) and (3), respectively. For brevity, we do not show the degraded I-V characteristic from sample 2. Figures S1 and S2 report the reverse-bias I-V characteristics as well. Further characterization of these novel heterojunction devices will be presented at the workshop.

IWGO-WeP-10 Temperature Dependent Hall as a Probe for Parasitic Conduction in Gallium Oxide Epitaxial Structures, Joshua Buontempo, Cameron Gorsak, Pushpanshu Tripathi, Hari Nair, Cornell University

$\beta\text{-Ga}_2\text{O}_3$ is a promising material for applications in radio frequency (RF) devices due to its ultra-wide bandgap ($\sim 4.8 \text{ eV}$) and estimated breakdown field strength of 8 MV/cm [1]. The δ -doping technique offers multiple advantages over bulk doping such as fine gate control of highly scaled devices [2]. Growth conditions must be tuned to achieve a sharp controlled doping profile exhibiting high channel mobility [2]. However, unintentional conduction pathways can complicate electrical characterization and obscure the intrinsic transport properties of the δ -doped channel. In this work, we leverage temperature-dependent Hall measurements to parse out the transport of unintentionally doped (UID) buffer layers from the Si δ -doped $\beta\text{-Ga}_2\text{O}_3$ epitaxial layers.

Samples with varying buffer layer thicknesses and carrier concentrations were grown by metalorganic chemical vapor deposition (MOCVD) on (010) $\beta\text{-Ga}_2\text{O}_3$ substrates. Temperature-dependent Hall measurements reveal anomalous carrier density behavior deviating from characteristic single-donor freeze-out. These trends are consistent with the presence of multiple conduction channels [3]. A structure with a sufficiently thin buffer, such that all carriers in the buffer should be fully depleted by the semi-insulating substrate, enables characterization of the δ -doped channel alone. By comparing samples with different buffer configurations, we identify that conductive buffer layers can significantly contribute to measured apparent transport.

These results demonstrate that parallel conduction impacts apparent δ -doped $\beta\text{-Ga}_2\text{O}_3$ transport properties and may lead to misinterpretation if not properly accounted for. These findings highlight temperature-dependent characterization as a method for identifying parasitic conduction pathways and provide insight into epitaxial design strategies for

isolating and optimizing the δ -doped channel in high-mobility β -Ga₂O₃ devices.

References

- [1] M. Higashiwaki, "β-Ga₂O₃ material properties, growth technologies, and devices: a review," AAPS Bulletin, vol. 32, no. 1, p. 3, 2022.
- [2] E. F. Schubert, ed., Delta-doping of Semiconductors. Boston, MA: Cambridge University Press, August 2005.
- [3] D. C. Look and R. J. Molnar, "Degenerate layer at GaN/sapphire interface: Influence on hall-effect measurements," Applied Physics Letters, vol. 70, pp. 3377–3379, 06 1997.

IWGO-WeP-11 3D Modeling of EFG β-Ga₂O₃ Crystal Growth: Effect of Process on Crystal Quality, Alex Galyukov, STR US, Inc.; Aleksa Crnobrnja, Andrey Smirnov, STR Europe, Serbia

Gallium oxide (β-Ga₂O₃) has emerged as a highly promising material for power electronics applications, owing to its wide bandgap (4.6–5.3 eV) and high critical breakdown electric field (~8 MV/cm) [1]. The edge-defined film-fed (EFG) growth technique is currently the preferred method for large-scale β-Ga₂O₃ crystal production, as it minimizes the melt free surface area, suppresses oxygen evaporation, and improves melt stoichiometry. Nevertheless, achieving large, high-quality crystals remains challenging due to stringent requirements for the lateral temperature uniformity, precise control of dopant incorporation and thermal stress distribution.

Numerical simulation has become an indispensable tool for understanding and optimizing the EFG growth process, enabling detailed analysis of physical phenomena that are difficult or impossible to access experimentally at the high process temperatures. In this work, we present a comprehensive conjugate 3D model of the EFG β-Ga₂O₃ growth system [2], developed using CGSim3D software. The model accounts for asymmetric features of the furnace geometry. It incorporates 3D temperature distribution throughout the furnace: radiative heat transfer in the semi-transparent crystal, including refraction and internal reflection at the crystal/gas interface. Model includes melt and gas flows with free surface tension and the Marangoni effect, dopant segregation and uniformity over the crystal, 3D thermal stress fields in the growing crystal.

We discuss the effect of modifications in furnace parameters on dopant incorporation uniformity and thermal stress development in the crystal. The results demonstrate practical approaches for optimizing growth conditions to reduce thermal stresses and minimize the risk of dislocation generation, improving yield and resistivity uniformity of β-Ga₂O₃ crystal.

Figure 1. Stress components in β-Ga₂O₃ crystal

Figure 2. Dopant distribution in the melt below the growth interface

- [1] M. Higashiwaki, et al., Appl. Phys. Lett. 100, 013504 (2012).
- [2] Y.-J. Shin et al., Jpn. J. Appl. Phys. 62, SF1022 (2023).

*Author for correspondence: Alex.Galyukov@str-soft.com

IWGO-WeP-12 Multi-Ribbon Growth of Offcut (100) β-Ga₂O₃ by EFG, Kurt Lindquist, David Joyce, Kale Geddis, Drew Haven, Luxium Solutions, LLC; Robert Lavelle, Luke Lyle, Benjamin Dutton, Penn State University

As wide-bandgap semiconductors such as SiC and GaN have seen increasing utilization in high-power applications due to their greater efficiency compared to traditional semiconductors, a search is underway for low-cost and high-efficiency alternatives to the currently available materials. Beta-phase gallium oxide (β-Ga₂O₃) is a promising candidate due to its superior material properties, such as an ultra-wide bandgap (~4.8 eV), high electric breakdown field (8 MV/cm), wide range of shallow *n*-type donors (e.g., Sn, Si, etc.), and excellent Baliga's figure of merit. In addition, β-Ga₂O₃ can be grown directly from the melt, unlike other wide-bandgap materials; this offers a path toward significant cost reductions in substrate manufacturing. However, development of β-Ga₂O₃ is still in the early stages and must overcome significant challenges to be manufactured at an industrial scale. Some notable challenges for bulk crystal growth of β-Ga₂O₃ are the low thermal conductivity and two facile cleavage planes of the β-Ga₂O₃ solid, both of which can prove difficult to overcome when scaling crystal size in three dimensions. Furthermore, the Ga₂O₃ melt decomposes to form

gallium metal, which attacks the iridium crucible and significantly reduces its lifetime.

At Luxium Solutions, we utilize the edge-defined film-fed growth (EFG) method for growth of β-Ga₂O₃ due to its unique ability to address the challenges enumerated above. Unlike many melt growth methods, EFG allows the crucible to be emptied of melt after each growth, preventing the buildup of gallium metal that leads to crucible decomposition. In addition, EFG allows for the growth of thin crystals (ribbons) that are effectively two-dimensional, allowing for substantial thermal transport through the crystal during growth despite its low thermal conductivity. However, iridium remains a large portion of the overall manufacturing cost, as it inevitably degrades from reaction with the oxygen required to suppress decomposition of the Ga₂O₃ melt. Therefore, techniques which can increase the yield of crystals from a single growth will significantly reduce manufacturing costs.

This presentation provides an overview of the development of EFG growth of β-Ga₂O₃ at Luxium Solutions, including an introduction to some of the challenges unique to β-Ga₂O₃. The discussion focuses on β-Ga₂O₃ EFG growth development over the last year, including simultaneous multi-ribbon growth, highlighting some of the challenges intrinsic to multi-ribbon growth and progress toward resolving those challenges. Through this discussion, we will demonstrate how this work enables the production of high-quality, domestically produced β-Ga₂O₃ substrates.

IWGO-WeP-13 Development of Surface Preparation Methods for Insulating and Conductive, Miscut (100) β-Ga₂O₃ Substrates, Robert Lavelle, Luke Lyle, Benjamin Dutton, Connor Beakes, Eric Welp, Scott Pistner, Andrew Balog, Penn State University; Drew Haven, David Joyce, Luxium Solutions; Nasim Alem, Joan Redwing, David Snyder, Penn State University

Encouraging epitaxial growth results on miscut (100) β-Ga₂O₃ substrates have motivated evaluation of this orientation for device applications. In addition to CMP, final substrate preparation is critical for facilitating high-quality epitaxial growth, especially for vicinal surfaces. Previous studies on insulating, Mg-doped substrates used phosphoric acid (H₃PO₄) etching and O₂ annealing steps prior to epitaxial growth. However, implementing this process resulted in significant surface roughening of Fe-doped substrates in this work. There is further motivation to utilize conductive substrates for higher power devices. These substrates also require alternative surface preparation steps as annealing in O₂ can result in passivation of the surface with Ga vacancies and a corresponding decrease in conductivity.

This study establishes surface preparation methods for both insulating, Fe-doped and conductive, Sn-doped miscut (100) β-Ga₂O₃ substrates. For both substrate types, an atomically smooth surface (Sq/rms <0.2 nm) with a uniform step/terrace structure was achieved by CMP followed by annealing at 850-900°C with a dwell time selected based on the miscut angle. For the Fe-doped substrates, reducing the total pressure was observed to be important for mitigating surface contamination with the optional inclusion of a hydrofluoric acid (HF) etching step (Fig. 1a). For the Sn-doped substrates, an epi-ready surface was also achieved by annealing in an inert, Ar atmosphere (Fig. 1b). Surface conductivity was maintained using a low O₂ partial pressure during annealing. However, Sn diffusion was observed, even at a relatively low temperature range, further emphasizing the importance of selecting appropriate surface preparation conditions for the miscut substrates. Overall, this study suggests that the surface ordering mechanism for miscut (100) β-Ga₂O₃ substrates is influenced by the Ga vacancy concentration and formation of defect complexes and/or diffusion via these sites. By controlling the variables that affect the formation/compensation of these vacancies, substrates can be prepared with vicinal surfaces for epitaxial growth.

IWGO-WeP-14 Composition-Dependent Thermal Conductivity of Ge_xSn_{1-x}O₂ Alloys, Xiao Zhang, Emmanouil Kioupakis, University of Michigan, Ann Arbor

GeO₂ is an emerging ultra-wide band gap semiconductor with strong potential for power electronic applications. Alloying GeO₂ with SnO₂, a well-established ultra-wide band gap material, enables tunability of material properties for device applications. Recent studies have demonstrated favorable electronic transport properties in Ge_xSn_{1-x}O₂ alloys, making them promising candidates for next-generation power electronics. However, the thermal conductivity, which directly controls heat dissipation and device reliability of these alloys, remains unexplored.

In this work[1] we investigate the thermal conductivity of Ge_xSn_{1-x}O₂ alloys as a function of composition and temperature using first-principles calculations. Density functional theory is used to determine the electronic

Wednesday Evening, August 5, 2026

structure, while density functional perturbation theory is applied to obtain phonon properties. The alloy is treated using the virtual crystal approximation while incorporating mass-disorder effects introduced by alloying. The phonon-limited thermal conductivity is then computed by solving the Boltzmann transport equation with the almaBTE software. Our results show that at room temperature, alloy disorder reduces directionally averaged thermal conductivity to values as low as 11 W/m K, i.e., by up to approximately a factor of four compared to the end compounds (41 W/m K for GeO₂ and 29 W/m K for SnO₂). Despite this reduction, the alloy thermal conductivity remains comparable to established ultra-wide band gap power-electronic materials such as Ga₂O₃. We further analyze the combined temperature and composition dependence of thermal transport, providing a compact function to evaluate thermal conductivity of Ge_xSn_{1-x}O₂. Our analysis of phonon mean-free-path distributions indicates that high quality crystalline samples with grain size of at least 400 nm are essential for reaching 80% of ideal thermal conductivity. Our work provides insights into the mechanisms that limit heat transport in Ge_xSn_{1-x}O₂ and offers predictive benchmarks for thermal conductivity to guide rational design of Ge_xSn_{1-x}O₂-based devices.

[1] X. Zhang and E. Kioupakis, Phys. Rev. Materials 9, 064603 (2025)

IWGO-WeP-15 MOCVD Growth and Characterization of β -Ga₂O₃ Field Effect Transistors Grown on 2" (010) Substrates, Will Brand, Fikadu Alema, Agniron Technology; Austin Hickman, Soctera; Andrei Osinsky, Agniron Technology

β -Ga₂O₃ has emerged as a promising material for next-generation power electronics due to its ultra-wide bandgap (~4.9 eV) and high theoretical breakdown field (~8 MV/cm). Among available deposition techniques, metal-organic chemical vapor deposition (MOCVD) has demonstrated strong potential for the growth of high-purity, low-defect β -Ga₂O₃ epitaxial films on native substrates [1]. The use of triethylgallium (TEGa) and trimethylgallium (TMGa) precursors enables the growth of carbon-free films with precise doping control. Resulting materials exhibit exceptional electronic properties, including low-temperature electron mobilities ranging from 10,000 to over 23,000 cm²/V·s and acceptor concentrations as low as 2×10^{13} cm⁻³, exceeding values reported for molecular beam epitaxy (MBE), hydride vapor phase epitaxy (HVPE), and even state-of-the-art SiC and GaN bulk materials [2,3].

This presentation will discuss the growth of β -Ga₂O₃ Field Effect Transistor (FET) structures on (010) substrates using Agniron Agilis 700 MOCVD system, supported by Agniron's SBIR program focused on the growth of FET structures on large area substrates. Growth of β -Ga₂O₃ using this reactor has shown both uniform growth on 2" and 4" substrates and uniform, low roughness surfaces across a 2" (010) substrates. To address parasitic conduction arising from the substrate/epitaxy interface, multiple buffer layer strategies were systematically investigated. While conventional HF pretreatment of the native substrate reduces interfacial silicon contamination, it is often insufficient to fully suppress the formation of a secondary conductive channel. Among the approaches explored, the most effective mitigation of interface charge was achieved through the implementation of a nitrogen-doped buffer layer with doping concentrations on the order of $6-8 \times 10^{18}$ cm⁻³, introduced via dilute NH₃/N₂ during growth. CV extracted N_a-N_a profiles indicate an average channel concentration of 1.6×10^{18} cm⁻³, with no measurable interface charge. Hall effect measurements show that carrier mobility remains comparable to unintentionally doped structures, with only a slight reduction in carrier concentration. A 22-point Hall mapping yields an average mobility of 104 cm²/V·s with a 1 σ non-uniformity of 1.5% across a 1" wafer. Thickness uniformity of 0.83% was achieved across a 2" wafer within the same growth run. Device-level performance, including transistor current density and threshold voltage characteristics, will also be presented.

[1] F. Alema, Journal of Crystal Growth 475, 77 (2017).

[2] G. Seryogin, Appl Phys. Lett. 117, 262101 (2020).

[3] F. Alema, APL Materials 7, 121110 (2019)

IWGO-WeP-16 DRCLS Defects Near LiGa₅O₈/Ga₂O₃ Heterointerfaces, Carlos DeLeon, Kaitian Zhang, Hongping Zhao, Leonard Brillson, Ohio State University

Lithium Gallate (LiGa₅O₈) is a novel semiconductor in high power electronics. In addition to a ~5.5 eV ultrawide bandgap (UWBG), LiGa₅O₈ exhibits p-type conductivity, which oxides like Gallium Oxide (Ga₂O₃) have difficulty achieving. Hence, lattice-matched LiGa₅O₈/Ga₂O₃ heterojunctions could enable UWBG P-N junctions, important for high-power electronics.

However, the novelty of LiGa₅O₈ also means that research to understand how its defects affect its electrical properties is still at an early stage.

Depth Resolved Cathodoluminescence (DRCLS) nanoscale depth analysis of LiGa₅O₈ films grown epitaxially on Ga₂O₃ measured its sub-bandgap optical emissions compared with theory [1] to understand their physical nature. DRCLS of LiGa₅O₈ on Ga₂O₃ revealed characteristic emissions of native defect complexes in both their heterointerface and Cr impurities.

DRCLS identified four primary defect emissions at 1.72 eV, 1.74 eV, 1.79 eV, and 1.84 eV. All four correlate to theoretical charge state transitions (CSTs) [1] and R1/R2 Cr defect features. TEM analysis suggested ~35 nm LiGa₅O₈ film thickness, while DRCLS depth profiles displayed pronounced defect intensity changes around ~50 nm, indicating interfacial-related defects. Thus both 1.72 eV and 1.84 eV defects are low within the LiGa₅O₈ but increase towards the substrate, while the 1.84 eV defect density increases near the free surface as well. Both the 1.74 and 1.79 eV defect features are dominant within the outer 60 nm, consistent with LiGa₅O₈ defects. For the 1.74 eV defect, first-principles CST calculations are consistent with Li_{Ga-tet}. [1] Its intensity decreases strongly but not entirely, extending into the Ga₂O₃ substrate whereas the 1.79 eV intensity decreases even more, indicating this defect is the LiGa₅O₈ film's most prominent defect. The closest CST indicates a Li_{Ga-tet}+Ga_{Li} complex, i.e., an exchange reaction, which is supported by the increased defect density being prominent in the Li rich film. The strong 1.84 eV emission at the free surface and the interface can be related to either a V_{Ga-oct} point defect based on a similar CST energy [1] for both LiGa₅O₈ and Ga₂O₃ or Cr features since Cr is an unintentional impurity in Ga source for both LiGa₅O₈ and Ga₂O₃.

DRCLS of LiGa₅O₈ and Ga₂O₃ heterointerfaces provide both measurement and physical nature of their defects, highlighting the impact of their buried interfaces on their nature and spatial distribution. Further refinement of both DRCLS technique and epitaxial growth of atomically abrupt interfaces are underway.

[1]Klichchupong Dapsamut, Kaito Takahashi, & Walter R. L. Lambrecht J. Appl. Phys. 135, 235707 (2024), <https://doi.org/10.1063/5.0209774>

IWGO-WeP-17 Electric-Field-Limited Breakdown in Oxide/ β -Ga₂O₃ p-n Heterojunction Diodes, Sanjay Gopalan, John Muth, Ki Wook Kim, North Carolina State University

Identifying a viable p-type partner for β -Ga₂O₃ is critical for enabling high-voltage bipolar devices. We evaluate oxide p-type candidates for β -Ga₂O₃ heterojunction (HJ) diodes by comparing NiO, Cr₂O₃, and GeO₂. Density functional theory (DFT) was used to extract band alignments for NiO/ β -Ga₂O₃, Cr₂O₃/ β -Ga₂O₃, and GeO₂/ β -Ga₂O₃. All interfaces exhibit type-II alignment with large valence-band offsets (>2 eV), enabling strong hole blocking and stable junction formation. Cr₂O₃ shows a slightly higher valence-band offset and comparable conduction-band offset to NiO, while GeO₂ exhibits moderate offsets that still support effective carrier confinement. Hybrid-functional fitting of bandgaps produces negligible change in predicted breakdown trends, confirming that device behavior is dominated by field distribution rather than small band-offset variations.

Using DFT-derived parameters, TCAD simulations were performed for NiO/ β -Ga₂O₃, Cr₂O₃/ β -Ga₂O₃, and GeO₂/ β -Ga₂O₃ HJ diodes. Owing to the absence of fully calibrated transport and impact-ionization models for β -Ga₂O₃, breakdown voltage (BV) is defined using a critical electric-field criterion of 8 MV cm⁻¹ in the Ga₂O₃ drift region. This provides a consistent comparative metric while β -Ga₂O₃ TCAD models remain under development. All heterojunctions demonstrate multi-kV blocking capability, with BV primarily limited by edge field crowding. Dielectric termination and field-plate structures redistribute the electric field and significantly enhance BV, with Cr₂O₃/ β -Ga₂O₃ showing slightly higher limits and GeO₂/ β -Ga₂O₃ exhibiting comparable trends under optimized designs.

IWGO-WeP-18 Hot-wall MOCVD Growth on Miscut (100) β -Ga₂O₃ Substrates, Benjamin Dutton, Robert Lavelle, Luke Lyle, Randal Cavaleiro, Connor Beakes, Scott Pistner, Penn State University Applied Research Laboratory; Drew Haven, David Joyce, Luxium Solutions LLC; David Snyder, Penn State University Applied Research Laboratory

Recent results in literature utilizing hot-wall metal organic chemical vapor deposition (HW-MOCVD) to grow β -Ga₂O₃ films have realized high growth-rates (>15 μ m/h) and low impurity incorporation. To date, these studies have mostly focused on (010) or (-201) commercially available substrates; however, films grown on miscut (100) β -Ga₂O₃ substrates by cold-wall MOCVD have encouraged further exploration into this orientation. In this study, HW-MOCVD is established as an effective method for epitaxial growth on (100) β -Ga₂O₃ substrates with miscut values ranging from 2° -

6°+ and doped with donors or acceptors using TMGa as a precursor. AFM scans indicated step-flow growth could be achieved at various miscut angles using the process parameters developed in this work. The effect of miscut angle on extended defect density and morphology was investigated using imaging techniques including optical microscopy and FIB-SEM. Process parameters, such as VI/III ratio, were also shown to demonstrably impact extended defect morphology. Background donor concentrations of the films were measured by Hg probe and SIMS in order to understand the impact of miscut angle on impurity incorporation. Lastly, growth conditions were modulated in pursuit of validating the homogeneity of HW-MOCVD over a 4-inch diameter platen area.

IWGO-WeP-19 Temperature-Optimized Lattice-Matched Epitaxy of UWBG Rutile $\text{Ge}_x\text{Sn}_{1-x}\text{O}_2$ on (001) Rutile TiO_2 , Satyam Patel, Becky (R.L.) Peterson, University of Michigan, Ann Arbor

r-GeO₂ is an emerging ultrawide bandgap (UWBG) semiconductor with predicted n- and p-type conduction, and with higher thermal conductivity and electron mobility than $\beta\text{-Ga}_2\text{O}_3$. [1] Alloying r-GeO₂ with r-SnO₂ forms r-Ge_xSn_{1-x}O₂, enabling tunable lattice parameters and bandgaps. [2] Lattice-matched r-Ge_xSn_{1-x}O₂/r-GeO₂ heterostructures are attractive for future electronic, optoelectronic, and quantum devices. While r-Ge_xSn_{1-x}O₂ epitaxy has been demonstrated on (001) r-TiO₂, [3, 4] the growth temperature has not been optimized. Here, we investigate the impact of growth temperature on stoichiometry and crystallinity of lattice-matched r-Ge_xSn_{1-x}O₂ films grown on r-TiO₂ via mist chemical vapor deposition (mist CVD).

In mist CVD, an ultrasonically-generated precursor mist flows into a furnace where it thermally decomposes on the substrate, forming a thin film. We used a 1 Ge to 1.21 Sn precursor ratio to target a Ge_{0.422}Sn_{0.578}O₂ alloy composition, which Vegard's law predicts will have relaxed in-plane lattice parameters matching (001) r-TiO₂. Eight samples were prepared with growth temperature varying from 725 °C to 900 °C. As growth temperature increased, the (002) 2 θ/ω peak shifted to lower angles, indicating an increased out-of-plane lattice parameter, *c*. Concurrently, the direct-forbidden transition energy redshifted from 4.03 eV to 3.77 eV, due to decreased Ge incorporation and changes in substrate-induced strain.

X-ray diffraction (XRD) reveals an optimal growth window between 750 °C to 775 °C, for which films exhibit the narrowest full width at half maximum (FWHM) in rocking curves and pronounced Laue oscillations in symmetric 2 θ/ω scans. The r-Ge_{0.43}Sn_{0.57}O₂ film grown at 775 °C demonstrated the highest growth rate (> 2 nm·min⁻¹), the lowest substrate-induced strain, sub-nanometer surface roughness, and superior structural quality, as shown in scanning transmission electron microscopy (STEM) imaging. Reciprocal space mapping, azimuth scans, and nanobeam electron diffraction (NBED) confirm lattice-matched epitaxy of the r-Ge_{0.43}Sn_{0.57}O₂ on TiO₂. In the future, these optimized growth conditions can be used to obtain high quality heterostructures in the Ge_xSn_{1-x}O₂ alloy system.

This work was supported by NSF DMR FuSe awards #2235208 and #2328701.

References: [1] S. Chae *et al.*, Appl. Phys. Lett. **114**(10), 102104 (2019); [2] A.M. Abed & R.L. Peterson, APL Mater. **13**(11), 111115 (2025); [3] H. Takane *et al.*, Phys. Rev. Mater. **6**(8), 084604 (2022); [4] H. Takane *et al.*, Appl. Phys. Express **17**(1), 011008 (2024).

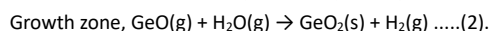
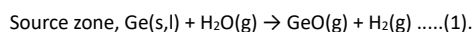
IWGO-WeP-20 Growth of Rutile-Type GeO₂ by Oxide Vapor Phase Epitaxy, Haru Nakano, Shigeyoshi Usami, Masayuki Imanishi, Yusuke Mori, Osaka University, Japan

Rutile-type germanium dioxide (r-GeO₂) has emerged as a promising power semiconductor material; however, achieving high material purity is essential to realize its full breakdown potential in device applications. Although various growth methods have been investigated, further improvements in material purity remain necessary. Recently, we proposed oxide vapor phase epitaxy (OVPE) as a novel technique for producing high-purity oxide thin films (e.g., Ga₂O₃). This method employs metal-oxide vapor as the source material, enabling intrinsically high-purity growth. In this study, we investigated OVPE to the growth of r-GeO₂. Growth was performed on a (001) r-TiO₂ substrate under conditions determined based on thermodynamic calculations. The formation of r-GeO₂ was confirmed through X-ray diffraction. Scanning electron microscope observations revealed thin-film growth, and cross-sectional SEM indicated a growth rate of approximately 200–500 nm/h. These results indicate that r-GeO₂ can be grown using the OVPE. However, an $\alpha\text{-GeO}_2$ polytype was also detected, and further investigation is required to clarify its origin.

IWGO-WeP-21 Thermodynamic analysis of GeO₂ growth via Oxide Vapor Phase Epitaxy, Shigeyoshi Usami, Masayuki Imanishi, Yusuke Mori, The University of Osaka, Japan

Rutile-type germanium dioxide (r-GeO₂) is one of the candidates for next-generation power semiconductor materials owing to its wide band gap (4.44-4.68 eV) [1], high breakdown electric field (~7 MV/cm) [2], and predicted ambipolar carrier conduction [3]. Although various thin-film growth methods for r-GeO₂ have been reported [4-6], the development of a high-purity growth technique, which is essential for achieving high breakdown voltage, is still required. Recently, we proposed oxide vapor phase epitaxy (OVPE) as a novel growth technique capable of achieving high-purity oxide thin films (e.g., Ga₂O₃) [7]. This method utilizes metal-oxide vapor as the source material, which is free from impurities originating from metal precursors and thus enables intrinsically high-purity growth. In this study, we investigate the feasibility of GeO₂ growth using OVPE through thermodynamic analysis.

In the OVPE method, metal-oxide vapor generated in the source zone is transported to the growth zone and mixed with an oxidant, resulting in the growth of a solid oxide on a substrate. The chemical reactions involved in GeO₂ growth are shown in Eqs. (1) and (2):



Thermodynamic equilibrium states were calculated by minimizing the Gibbs free energy under given conditions of temperature, partial pressures, and total pressure. First, the temperature dependence of the equilibrium partial pressure (P_{eq}) of GeO(g) and the H₂O-to-GeO conversion efficiency in the source zone were evaluated. The amount of GeO(g) increases with source-zone temperature, and a temperature above 1000 °C is required to achieve a conversion efficiency greater than 90%.

Next, the temperature dependence of the supersaturation for GeO₂ growth at various H₂O partial pressures was evaluated. The supersaturation was derived from the difference between the initial and equilibrium partial pressures of GeO(g). The temperature range for GeO₂ growth expands with increasing H₂O partial pressure. Comparison with growth temperatures employed in other methods suggests that the rutile phase is achievable by OVPE.

- [1] M. Stapelbroek *et al.*, Solid State Commun. **25**, 959-962 (1978).
- [2] K. Bushick *et al.*, Appl. Phys. Lett. **117**, 182104 (2020).
- [3] S. Chae, J. Lee *et al.*, Appl. Phys. Lett. **114**, 102104 (2019).
- [4] H. Takane *et al.*, Appl. Phys. Lett. **119**, 062104 (2021).
- [5] K. Shimazoe *et al.*, Jpn. J. Appl. Phys. **64**, 050903 (2025).
- [6] F. Golbasi *et al.*, J. Alloys Compd. **1014**, 178591 (2025).
- [7] R. Togashi *et al.*, DOI: 10.35848/1347-4065/ae54ed.

IWGO-WeP-22 Experimental Study of Hf-Doped $\beta\text{-Ga}_2\text{O}_3$ by Floating Zone Method, Myeonggyun Kang, Tohoku University, Japan, Republic of Korea; Kei Kamada, Hisato Suezumi, Masanori Kitahara, Satoshi Ishizawa, Kikito Murakami, Yuui Yokota, Masao Yoshino, Akira Yoshikawa, Tohoku University, Japan

Introduction: Czochralski (Cz) and Edge-Defined Film-Fed Growth (EFG) methods inevitably require the use of expensive Ir crucibles and, as the market price of Ir rises, there is a strong demand for economically viable alternatives [1]. Here, our laboratory has proposed the Oxide Crystal Growth from Cold Crucible (OCCC) using the raw material itself as the crucible [2]. However, since OCCC is designed for large-scale experiments, it is not suitable for composition screening; therefore, in this study, we used Floating Zone (FZ) method. According to DFT calculations, Hf forms a shallow donor level within $\beta\text{-Ga}_2\text{O}_3$ and Saleh *et al.* (2020) reported high carrier density in Hf-doped $\beta\text{-Ga}_2\text{O}_3$ grown by VGF method [3][4]. However, no studies have yet been reported on the growth of Hf-doped $\beta\text{-Ga}_2\text{O}_3$ single crystal using FZ. In addition, the report on optical properties of Hf-doped $\beta\text{-Ga}_2\text{O}_3$ are very few. In this study, we grew Hf-doped $\beta\text{-Ga}_2\text{O}_3$ single crystals using FZ and report on their optical and electrical properties.

Experiments: $\beta\text{-Ga}_2\text{O}_3$ and HfO₂ powder were uniformly mixed by milling with HfO₂ doping with various concentrations. During the crystal growth, the rotation rate was set to 30 rpm, and the vertical pull-down rate was 6 mm/h in 100% O₂.

Results: Non-doped and Hf-doped $\beta\text{-Ga}_2\text{O}_3$ single crystals with a diameter of 4-5 mm were successfully obtained. Under UV light (254 nm) irradiation, the non-doped sample exhibited blue luminescence, whereas green luminescence was observed in the Hf-doped sample. Furthermore, in the PL spectra measured at 280 nm excitation, the Hf-doped sample showed broader emission and peak shift to 460 nm, compared to the non-doped

sample. Results such as XRD, and Hall effect measurements etc. will be reported on the day of the presentation.

Acknowledgements: We appreciate Takamasa Sugawara, Cooperative Research and Development Center for Advanced Materials, providing access to the Floating Zone Furnace.

[1] S. B. Reese, et al., *Joule* 3, 903-907 (2019)

[2] A. Yoshikawa, K. Kamada et al. *Sci. Rep.* 14, 14881 (2024)

[3] D. Chen et al. *Comput. Theor. Chem.*, 1241, 114906 (2024)

[4] M. Saleh et al., *Semicond. Sci. Technol.*, 35, 04LT01 (2020)

* Author for correspondence: akira.yoshikawa.d8@tohoku.ac.jp

IWGO-WeP-23 Exploration of Conductivity-Type Control in β -Ga₂O₃ through Nitrogen Doping, Haizhong Zhang, Fuzhou University, China

β -Ga₂O₃ is a next-generation ultra-wide-bandgap semiconductor with strong potential for power electronics and deep-ultraviolet photodetection owing to its ultra-wide bandgap and high critical breakdown field. However, its device performance remains far below the theoretical limit because intrinsic materials limitations, particularly the flat valence band and strong self-compensation induced by unintentional donors, continue to hinder precise control of epilayer quality and reliable p-type doping. Among the candidate dopants, nitrogen (N) is particularly attractive because its atomic radius is close to that of the host anion, making it a favorable compensating acceptor with minimal perturbation to the O²⁻ sublattice. To explore a viable route toward p-type β -Ga₂O₃, we adopted a strategy of first establishing high-quality epitaxial growth and then pursuing carrier control, and systematically investigated in situ N doping in β -Ga₂O₃ homoepilayers grown by metal-organic chemical vapor deposition (MOCVD). Using nitrous oxide (N₂O) as both the oxygen precursor and nitrogen source, together with trimethylgallium as the Ga precursor, we first suppressed unintentional donor incorporation through process optimization. This enabled the growth of a lightly N-doped layer on (001) β -Ga₂O₃ with a low background carrier concentration of $3.5 \times 10^{16} \text{ cm}^{-3}$ and a high electron mobility of $82.70 \text{ cm}^2 \text{ V}^{-1} \text{ s}^{-1}$. By further precisely regulating N incorporation, we drove the (001) homoepilayer from n-type conduction through a highly resistive state to p-type conduction, thereby obtaining a room-temperature p-type epilayer with a hole concentration of $1.08 \times 10^{18} \text{ cm}^{-3}$, a hole mobility of $0.47 \text{ cm}^2 \text{ V}^{-1} \text{ s}^{-1}$, and an acceptor activation energy of 0.168 eV. By combining first-principles calculations with experimental results, we further revealed an orientation-dependent N-doping mechanism on the (001) and (100) planes, arising from differences in the competitive adsorption of N and O on the two surfaces. The results show that the (001) plane is more suitable for precise control of N incorporation, whereas the (100) plane is more favorable for high-concentration N doping. Guided by this understanding, we further achieved precise in situ N doping on the (100) plane and obtained a homoepilayer with an N concentration as high as $1.13 \times 10^{20} \text{ cm}^{-3}$. Multiple Hall measurements together with Seebeck measurements confirmed p-type conduction, with a hole concentration of $9.15 \times 10^{18} \text{ cm}^{-3}$ and a hole mobility of $1.43 \text{ cm}^2 \text{ V}^{-1} \text{ s}^{-1}$.

IWGO-WeP-24 Re-Growth on Multi-Directional Fin Structures of (001) β -Ga₂O₃, Sai Kkrishna Anandan, Min-Yeong Kim, Arpit Nandi, Martin Kuball, University of Bristol, UK

Homoepitaxial growth of β -Ga₂O₃ focuses on conventional vertical growth on commercially available substrate orientations such as (001), (010), (201) and (110) [1]. Exploring lateral epitaxial growth, though limited, could increase the ability to design and implement new device structures, e.g. gate-all-around FETs, that benefit from anisotropy in electron transport and heat propagation within the β -Ga₂O₃ monoclinic structure. This work investigates the growth of β -Ga₂O₃ along the vertical sidewall of fins fabricated into (001) β -Ga₂O₃ substrates, along multiple in-plane directions like [010], [100], [140], [120], [110], [210], and [210]. The result shows anisotropy of regrowth surfaces depending on the crystallographic orientations of RIE etched side walls. Fig. 1(a) and Fig. 1(b) show FIB-SEM cross-sectional images along the [120] directional fin before and after growth, respectively, at a growth rate of 500 nm/h (vertical direction) for 30 mins at 930°C, 30 Torr, and a VI/III ratio of 1800. The increase in fin thickness on the fin side walls in Fig. 1(b) is used to assess the lateral growth rate on the sidewall. Fig. 1(c) represents the change in overgrowth thickness along the different sidewalls of fins under identical growth conditions. The highest lateral growth was observed along [140], [120], and [210] directional fins, exhibiting 50% of the vertical growth rate along (001). This variation is likely caused by anisotropy in atomic density on the sidewall planes leading to varying surface energies for nucleation. H₃PO₄ surface treatment has been proven to reduce

interface charge density (mitigating current degradation) in Trench Schottky Barrier Diodes and an increased stability of the device under high temperature operation [2]. Hence, regrowth on 10 min and 20 min H₃PO₄-treated side wall surfaces was compared to an untreated regrowth surface. Fig. 1(c) shows that H₃PO₄ treated samples (10 mins) exhibit reduced growth compared to the untreated surface on most surfaces apart of side walls is (010) fins; acid treatment may cause a reduction in nucleation sites and adsorption centers hindering growth kinetics [3].

IWGO-WeP-25 Surface Termination and Structural Stability of β -(Al_xGa_{1-x})₂O₃ (X = 0 ~ 0.3) as-Cleaved Single Crystals, Ming-Chao Kao, Deutsches Elektronen-Synchrotron DESY (NanoLab), Germany

As demonstrated in our recent publication on APL [1] The surface structure of β -Ga₂O₃ single crystals cleaved along the (100) plane is investigated using synchrotron-based surface X-ray diffraction (SXRD) and atomic force microscopy (AFM). The results show the surface to consist of a single, so-called B-termination, which means that the crystal cleaves at planes formed by edge-sharing oxygen octahedra, thereby breaking the longest and weakest Ga–O bonds. Refinement of the atomic positions results in small displacements from the bulk structure, at most approximately 0.01 Å. AFM suggests that relatively large terraces form together with steps of half the a-axis length of approximately 0.6 nm, which means that terraces have the same atomic termination, related by the crystal symmetry. These results are important as a fundamental property of β -Ga₂O₃ when processed or used in various high-power semiconductor applications.

Building on our recent structural characterization of the cleaved β -Ga₂O₃ (100) surface, we now present initial results from synchrotron-based single-crystal X-ray diffraction (SCXRD) and X-ray reflectivity (XRR) measurements of β -(Al_xGa_{1-x})₂O₃ (100) single crystal substrates (x = 0 to 0.3). [2] These measurements provide new insight into the surface structure and bulk crystal properties of these Al-alloyed single crystals, which are critically important for high-quality epitaxial thin-film growth. Our results provide a comprehensive analysis of the lattice parameters, electron density, Al compositions, twinned domain, and surface structure of the alloyed β -(Al_xGa_{1-x})₂O₃ crystals. Furthermore, we propose several structural models, suggested by first-principles studies [3] and our PXRD-refined bulk model, which were subsequently used to fit the Crystal Truncation Rod (CTR) dataset and will reveal the key surface structural features of these alloyed single crystals. These findings will be discussed in detail at the conference. All investigated β -(Al_xGa_{1-x})₂O₃ single crystals shown in this study were grown using the Czochralski method at the Leibniz-Institut für Kristallzüchtung (IKZ). [2]

[1] Kao, Ming-Chao, et al., *Applied Physics Letters* 128.7 (2026).

[2] Galazka, Zbigniew, et al., *Journal of Applied Physics* 133.3 (2023).

[3] Mu, Sai, et al., *APL Materials* 8.9 (2020).

* Author for correspondence: vedran.vonk@desy.de

IWGO-WeP-26 Effect of the GaN Surface on n-Ga₂O₃/p-GaN Heterointerface Quality, Daniel Pennachio, US Naval Research Laboratory; Frank Kelly, Katie Gann, National Research Council Postdoctoral Fellow, residing at NRL; Emma Rocca, Michael Mastro, US Naval Research Laboratory

Gallium oxide is a promising ultrawide bandgap semiconductor due to its phenomenal electrical properties such as its high breakdown field and n-type conductivity. Importantly, compatibility with liquid-phase growth techniques allow large-area β -Ga₂O₃ substrates to be produced relatively inexpensively and early in the material's development. Despite these benefits, the lack of shallow p-type dopant and the material's low thermal conductivity hinder device performance. Both disadvantages may be resolved by forming heterostructures with compatible p-type semiconductors. This work explores epitaxy of n-type β -Ga₂O₃:Si via metalorganic chemical vapor deposition (MOCVD) on p-type GaN:Mg, with a focus on atomic configuration and associated defects of the heterointerface as a function of Ga₂O₃ growth initiation and substrate polarity.

This work investigates the effect of GaN surface modifications before Ga₂O₃ growth. Surface treatments include *ex situ* O₂ plasma oxidation or an *in situ* MOCVD Ga "flash" clean of the GaN surface [1]. The effects of the polarity of the GaN substrate and the inclusion of a low-temperature Ga₂O₃ nucleation layer are also studied in addition to the surface treatments. The interfacial structure and composition were measured using scanning transmission electron microscopy (STEM) and X-ray energy dispersive

Wednesday Evening, August 5, 2026

spectroscopy (EDS). All grown films exhibited rotational domains with the epitaxial alignment of $\text{Ga}_2\text{O}_3(-201)||\text{GaN}(0001)$. A 6-fold rotational alignment between the substrate and film were confirmed via X-ray diffraction (XRD). Fourier filtering and 4DSTEM were utilized to map grain alignments throughout the cross-sections, showing both vertical and horizontal grain boundaries, as well as various other defects. Predominant crystallographic alignments observed were $\text{Ga}_2\text{O}_3(-201)(0-10)||\text{GaN}(0001)[11-20]$ and $\text{Ga}_2\text{O}_3(-201)[1-32)||\text{GaN}(0001)[11-20]$. The film grown with *ex situ* oxidation but without a nucleation layer provided the largest lateral grain size as determined via atomic force microscopy (AFM) analysis of surface structure. This growth also exhibited relatively uniform lateral grain size throughout the film thickness in TEM. In contrast, films grown with a nucleation layer resulted in smaller lateral grain sizes near the interface, followed by wider grains near the film surface. For samples treated with *ex situ* oxidation, the interface showed a ~ 10 nm wide region containing voids, while samples grown without oxidation showed atomically abrupt interfaces.

[1] Katta, Abishek, et al. *Journal of Applied Physics* 135.7 (2024).

IWGO-WeP-27 p-GaN/n-Ga₂O₃ Diodes via MOCVD Selective Area Growth, Frank Kelly, Emma Rocco, Daniel Pennachio, James Lundh, Alan Jacobs, Tolen Nelson, Marko Tadjer, Michael Mastro, Naval Research Laboratory
Heteroepitaxy of n-Ga₂O₃ on p-type wide-bandgap semiconductors is a promising route for high-performance power rectifiers. Here we demonstrate p-GaN/n-Ga₂O₃ heterojunction diodes fabricated via MOCVD-based selective area growth. PECVD SiN_x was used as the growth mask material to enhance the surface diffusivity of Ga adatoms and prevent nucleation of polycrystalline material on the mask, a common issue with traditional SiO₂ masks. SiN_x layers were 90 nm thick and were patterned via wet etching with BOE. Growth was conducted at 800 °C with a growth pressure of 15 Torr and VI/III ratio of 890 in an Agnition Agilis 500 MOCVD reactor. SiH₄ was used as an n-type dopant source for Si. Growth temperature, pressure, and VI/III ratio were identified as important parameters to optimize to prevent polycrystalline Ga₂O₃ nucleation. Devices were fabricated by depositing Ti/Au contacts to the Ga₂O₃ and Pd/Au contacts to the p-GaN. Devices were tested in air prior to contact annealing and without passivation.

The fabricated diodes exhibit record-breaking performance of Ga₂O₃ devices produced via MOCVD-SAG, with current on/off ratios exceeding 10⁹ and the reverse bias current limited by the noise floor of the measurement system. Ideality values were around 3.5 and forward specific on resistance was high, suggesting improved performance can be obtained through contact annealing. Breakdown voltages were measured to be 50 V reverse bias for a 10 μm contact spacing, indicating breakdown through air rather than through the device. Mesas were non-uniform in thickness and doping due to excess unreacted Ga from the mask accumulating in growth windows. Plan-view scanning electron microscopy (SEM) of the device edge shows that the mask does not have crystallites and that the mesa edge has hexagonal faceting, attributed to the 6-fold rotational domains that β-Ga₂O₃ forms on c-plane GaN. Cross-sectional SEM shows lateral overgrowth and an increased thickness near the mask edge. Further study of the variation in doping level and its impact on device performance will be carried out and presented at the workshop.

*Author for correspondence: frank.p.kelly9.ctr@us.navy.mil

IWGO-WeP-28 Performance of MOCVD Grown Schottky Barrier Diodes with a Graded β-(Al,Ga)₂O₃ Cap, Cameron Gorsak, Frank Kelly, Jenifer Hajzus, Daniel Pennachio, Naval Research Laboratory; Katie Gann, Naval Research Laboratory, USA; Alan Jacobs, Emma Rocco, Michael Mastro, Naval Research Laboratory

β-Ga₂O₃ with its high critical electric field (E_{cr}) and controllable n-type doping, is an advantageous material for Schottky barrier diodes (SBDs) for compact, high-voltage, power conversion and distribution systems. A common failure mechanism in SBDs is electric field breakdown at the metal-semiconductor interface, where the field peaks under reverse bias. To further improve SBD performance, this work employs a β-(Al,Ga)₂O₃ cap, which provides a larger bandgap (E_g) and a correspondingly higher E_{cr} [1]. The corresponding decrease in electron affinity is predicted to increase the Schottky barrier height (Φ_b) to high work function metals. Previous work has demonstrated that a β-(Al,Ga)₂O₃ cap enhances SBD device performance by suppressing reverse leakage current via a higher Φ_b while simultaneously increasing the breakdown voltage (V_{br}) due to a higher E_{cr} [2]. The abrupt heterojunction, however, resulted in higher on resistance (R_{on}). To retain the benefits from the wider bandgap cap while minimizing

R_{on} , this work investigates the metalorganic chemical vapor deposition (MOCVD) of a compositional graded β-(Al,Ga)₂O₃ capped SBD.

An Agnition Agilis 500 MOCVD reactor is used to grow the UID drift region and graded β-(Al,Ga)₂O₃ cap on (010) Sn:β-Ga₂O₃ substrates using TEGa and O₂ precursors. The flow of TMAI is ramped to achieve the linearly graded β-(Al,Ga)₂O₃ layers. While the critical thickness for a commensurate, abrupt 20% β-(Al,Ga)₂O₃ film is limited to ≤ 30 nm [3], compositional grading offers a pathway to achieve higher Al content by distributing strain. This work presents a parametric investigation into the surface content of graded β-(Al,Ga)₂O₃ caps, including targeted compositions of 10%, 20%, and 30%. The initial device features a crack-free, ~ 15 nm graded cap with a surface Al content of $\sim 10\%$, as confirmed by scanning transmission electron microscopy energy dispersive X-ray spectroscopy. Both uncapped and capped surfaces exhibit as-grown roughness as low as ~ 1 nm RMS.

SBDs with 500 μm diameter Pt/Au Schottky contacts and backside Ti/Au ohmic contact are fabricated on the wafers. Results indicate that the β-(Al,Ga)₂O₃ devices exhibit a higher reverse V_{br} while maintaining a low R_{on} ≈ 0.01 Ωcm², comparable to the uncapped devices. This demonstrates the effectiveness of the graded cap in improving blocking performance without significantly increasing conduction losses. A direct comparison of key device parameters, including R_{on} and leakage current, will be presented.

References:

- [1] H. Peelaers et al., *APL* **112**(24), (2018).
- [2] P. Sundaram et al., *JVSTA* **40**(4), (2022).
- [3] J.S. Lundh et al., *APL* **123**(22), (2023).

IWGO-WeP-29 Vertical β-Ga₂O₃ U-Trench MOSFETs With N-ion-implanted Current Blocking Layer and Implanted Source, Jiawei Liu, Surajit Chakraborty, Walid Amir, Uttam Singiseti, University at Buffalo-SUNY

β-Ga₂O₃ has attracted significant attention as an ultra-wide-bandgap (UWBG) semiconductor for next-generation high-power and fast-switching. Among diverse device architectures, vertical MOSFETs are preferred in power electronics for their ability to mitigate surface effects and achieve scalable breakdown voltage (V_{br}) through drift layer thickness scaling. To compensate for the absence of p-type doping in Ga₂O₃, forming fin-type structures or introducing a current blocking layer (CBL) are the main methods to realize normally-off operation. Considering the requirement of high lithography resolution for fin structures, the CBL approach is investigated in this work.

The fabrication process started on commercially available Sn-doped (010) β-Ga₂O₃ substrates and ~ 10 μm HVPE-grown epitaxial layer with a doping concentration of $\sim 2 \times 10^{16}$ cm⁻³. The box-shaped CBL with a thickness of approximately 800 nm was formed by N-ion implantation at multiple energy levels with specific doses. Afterward, the sample was annealed in an N₂ ambient to activate nitrogen ions and remove ion implantation damage. To form ohmic contacts, Si-ion implantation was then performed with a PECVD SiO₂ sacrificial layer to form a 0.2-μm-thick box profile followed by anneal in N₂ atmosphere. Ti/Au was then deposited on the front and backside, followed by anneal in N₂. The gate trench and mesa isolation regions were etched in BCl₃/Ar-base RIE and a SiO₂ layer was deposited by ALD as the gate dielectric layer, followed by gate metallization.

To analyze device behavior, the ohmic contact was first characterized, yielding a contact resistivity of 1.94×10^{-6} Ω·cm² and sheet resistance of 555.63 Ω/□ by CTEM measurements. Threshold voltage $V_{th} = 3.8$ V and the on/off ratio of 7.0×10^2 were extracted from the transfer characteristics measured at $V_{DS} = 5$ V. From the output characteristics, the highest current density of 50.0 A/cm² was obtained at $V_{GS} = 15$ V and $V_{DS} = 4$ V and the on resistance ($R_{on,sp}$) was extracted to be 56.9 mΩ·cm². Turn-on capacitance–voltage (C–V) measurements indicates sufficient gate control. However, the off-state C–V characteristics reveal the premature depletion of the drift layer. Breakdown measurements were performed at $V_{GS} = 0$ V and got a V_{br} of 342 V. The low V_{br} along with the low on/off ratio and the early depletion of the drift layer indicates the leakage issue in the CBL possibly caused by Si ion diffusion.

This study demonstrates an enhancement-mode β-Ga₂O₃ U-trench MOSFET with N-ion-doped CBL. Further optimization of the ion implantation, post-implantation annealing and the trench etching could be explored to solve the leakage.

IWGO-WeP-30 Donor Doping of β -Ga₂O₃ by Cl Ion Implantation, Katie Gann, Alan Jacobs, Frank Kelly, Emma Rocco, Cameron Gorsak, Marko Tadjer, Naval Research Laboratory; Rachael Myers-Ward, Naval Research Laboratory; Karl Hobart, Michael Mastro, Naval Research Laboratory

N-type doping in β -Ga₂O₃ has focused on substitutional impurities on Ga sites, such as Si. Chlorine substitution on O sites was proposed as a shallow donor, along with F,[1] in 2010 but has not been experimentally verified. To investigate Cl as an intentional donor, 500 nm UID β -Ga₂O₃ films grown by MOCVD on semi-insulating (010) substrates were implanted with either Si, Cl, or Si+Cl (at a 2:3 ratio to match the stoichiometry of Ga₂O₃) to concentrations of roughly 2×10^{19} , 3×10^{19} , and 5×10^{19} cm⁻³, respectively, to ~250 nm deep. Strain in the 020 XRD reflection of as-implanted samples varies for the different species and does not appear additive for the Si+Cl sample. Annealing was performed under a UHP Ar ambient at a reduced total pressure with P_{O₂}, P_{H₂O} < 10⁻⁶ bar, as both are known to be detrimental to activation of implanted Si, and likely for all n-type donors.[2]

Implant activation of Si served as baseline, where annealing for 10 minutes at 900, 925, and 950 °C yielded nearly full activation (~90%) with a mobility of ~60 cm²/Vs, confirming conditions are well optimized for Si implants compared to literature.[2] The Cl implanted samples exhibited increasing conductivity with temperature, not attributable to a change in mobility (~58 cm²/Vs), but rather to carriers increasing from ~2 to 10% of the implanted dose. The constant mobility suggests the increase in activation with temperature is likely not due to improved lattice recovery, with HRXRD confirming significant damage recovery by 900 °C. Literature suggests that implant damage primarily impacts the Ga sublattice, with the O sublattice remaining largely unperturbed. This may explain why dopants intended for Ga sites activate at relatively low temperatures, because Ga vacancies are formed via implant damage. However, for dopants intended for O sites to become active, higher annealing temperatures may be required for solute substitution. An activation energy of 2.1 eV from Cl activation anneals may be related to the formation of V_O necessary for Cl substitution. Temperature-dependent Hall measurements of the Cl-implanted samples (200-380K) reveal a carrier activation energy of ~12 meV, suggesting that a shallow impurity band was formed. Activation of the Si+Cl implanted samples show reduced activation and mobility compared to the Si-implanted samples, highlighting complicating factors from substituting on both sublattices and potentially the formation of compensating acceptors with the higher donor concentration.

[1] Varley, J. B., et al, (2010). *Applied Physics Letters*, 97(14).

[2] Gann, K. R., et al, (2024). *Journal of Applied Physics*, 135(1).

IWGO-WeP-31 Thermodynamic analysis of (Al_xGa_{1-x})₂O₃ MOCVD growth with TMA, O₂, and TMG and TEG as Ga precursors, Andri Dhora, Lund University, Sweden

Incorporating Al in β -Ga₂O₃ enhances its critical electric field and voltage-blocking capability. High quality, high purity β -(Al_xGa_{1-x})₂O₃ films with precise compositional control are required. MOCVD is a promising method for this goal [1], but challenges persist in achieving high growth rates while maintaining controlled conductivity and Al incorporation.

Numerous studies on MOCVD (Al_xGa_{1-x})₂O₃ growth are available, but clear guidelines for optimal conditions enabling high-purity and controlled Al incorporation are still lacking. We address this by performing a thermodynamic analysis of reactions between MO alkyls and O₂ during alloy growth with TMA, and either TEG or TMG as Ga precursors. For TEG, equilibrium partial pressures of 28 gaseous species were calculated from 24 chemical reactions and 4 constraints. For TMG, 29 gaseous species were analysed using 25 reactions and 4 constraints. These equilibrium partial pressures capture the reaction dynamics and clarify (Al_xGa_{1-x})₂O₃ growth behavior as a function of temperature, pressure, precursor supply, VI/III ratio, and the input gas-phase Al fraction (x_o).

The analysis shows that sufficient O₂ is required to fully combust MO-derived hydrocarbons and H₂, enabling high-purity growth at high rates. The required VI/III ratios differ as the precursors have different alkyl ligand compositions: above (21-x_o) for TEG and above 12 for TMG. In oxygen-rich regimes, the alloy composition (x) scales linearly with input Al fraction, whereas higher temperatures and oxygen-lean conditions enhance Al incorporation with an inverse dependence on VI/III ratio. Experimental data are well-reproduced by the thermodynamic model when accounting for differences in the kinetic growth efficiencies of the binary components under TMG and TEG; however, the TMG data points at higher TMA flow rates can be reproduced by assuming gas-phase losses, resulting in reduced effective precursor partial pressures at the growth interface.

[1] Bhuiyan, A.F.M., et al, *Journal of Applied Physics*, 133(21) (2023).

Wednesday Evening, August 5, 2026

+ Author for correspondence: andri.dhora@fysik.lu.se
[mailto:andri.dhora@fysik.lu.se]

IWGO-WeP-32 Effect of Ga Etching and Wet Acid Treatments on MOS Characteristics for Vertical β -Ga₂O₃ Power Devices, Akhila Mattapalli, Chinmoy Nath Saha, University of California at Santa Barbara; Carl Peterson, Steve Rebollo, Jim Speck, Sriram Krishnamoorthy, University of California Santa Barbara

Understanding the impact of trench/fin processing on MOS characteristics is key for realizing low-leakage, high field strength dielectrics for vertical trench diodes and transistors. We report on MOCVD Ga etching and wet chemical treatments (HF, HF & HCl, HF & heated H₃PO₄ (HP)) implemented on β -Ga₂O₃ trench structures and their effect on MOS leakage, breakdown and interface charge trapping. Gallium Oxide trenches of 2 or 5 μ m widths were fabricated with a footprint of 200 x 200 μ m² or 300 x 300 μ m² using a BCl₃ ICP-RIE dry etch process or TEGa Ga etch utilizing an MOCVD reactor (25 μ mol/min, 15 Torr, 800°C). We patterned [010] trenches with (100) sidewalls to minimize dry etch damage. The devices were fabricated on a 10 μ m (001) HVPE grown 10¹⁶ cm⁻³ doped drift layer on a Sn-doped conducting substrate. Planar MOS pads were also fabricated on the etched surface to distinguish between planar and sidewall leakage. After the trench etch (dry or Ga), the dry etched surfaces were treated with HF, HF & HCl, or HF & HP, and the Ga etch sample was treated with HF to remove the hard mask. Following trench definition and treatments, 55 nm Al₂O₃ gate oxide was deposited using plasma ALD, followed by Mo metal deposition. PR planarization was used to define the sidewall gate metal length. These steps were modeled after a typical vertical FinFET process. Current-voltage (J-V), capacitance-voltage (C-V), C-V hysteresis, reverse and forward breakdown measurements were carried out to characterize the trench MOS and planar MOS test structures.

All four samples had low baseline leakage (10⁻⁶ A/cm²), but the HF & HP and Ga etch samples had lower leakage compared to the HF and HF & HCl treated samples under higher forward voltage. C-V hysteresis measurements with a 5-min accumulation stress displayed reduced charge trapping in the Ga etch sample compared to the treated dry etch samples for planar MOS structures. The average trapped charge in the planar samples was 2.7, 6.3, 4.2, and 2.0 x 10¹¹ cm⁻² for Ga etch, HF & HP, HF, and HF & HCl respectively. The trench devices had similar trends, including a large device-to-device variation for the HF & HCl and HF samples. A 1.4 kV catastrophic breakdown was observed for the HP sample and 1.3 kV for the Ga Etch sample. An oxide breakdown field of 6.3 MV/cm was measured using forward I-V characteristics for Ga Etch planar samples with a 55 nm gate oxide. This study indicates that dry etch followed by heated H₃PO₄ treatment and trench etch using Ga precursor are promising approaches to realize low-leakage, high breakdown, low interface state density MOS junctions for vertical trench diodes and vertical transistors.

IWGO-WeP-33 High-Temperature Stability of Contacts to β -Ga₂O₃, Donivan R. Mouch, The Applied Research Lab at The Pennsylvania State University; Paul Kelemen, Sohyun Lee, Nathan S. Banner, Chan-Wen Chiu, Suzanne E. Mohney, Pennsylvania State University; Luke A. M. Lyle, The Applied Research Lab at The Pennsylvania State University

β -Ga₂O₃ is among the most promising candidates to replace Si in power electronics as it features an ultrawide band gap, shallow n-type dopants, and a large Baliga's figure of merit. It has the potential to surpass both SiC and GaN as a material for high power electronics due to the above considerations and presents the potential for scaling up manufacturing due to its ability to be grown from the melt. Wide and ultra-wide band gap semiconductors, like β -Ga₂O₃, offer the ability to operate at high voltages, high power, and high temperatures (> 300 °C). However, promising aspects of β -Ga₂O₃ can be limited, in part, due to the metal/semiconductor interface when high operating temperatures are required. The work examines the metallurgical stability of metallizations at elevated temperatures up to 700 °C.

This work explores the popular Ti/Au 20/100 nm and new Ti/TaSi₂/Ti/Pt 20/150/5/100 nm ohmic contacts for high-temperature applications. Ohmic contacts are annealed for 60 s at 100 °C increments in a rapid thermal annealing furnace, starting at 300 °C and increasing until failure. As deposited and annealed contacts are probed to determine specific contact resistances using the Cox-Strack method. In this work we demonstrated that by using the new Ti/TaSi₂/Ti/Pt ohmic contact, we can achieve a lower specific contact resistance by more than a factor of two after annealing at 500 °C. In addition to offering lower specific contact resistances, the Ti/TaSi₂/Ti/Pt ohmic contact continues to improve upon further annealing

up to 700 °C, while the Ti/Au contact is longer usable. We think that the failure mechanism of the Ti/Au, at 700 °C, may in part be caused by agglomeration of the Au layer. In addition, we will also present work on high-temperature stability of Schottky diodes to β -Ga₂O₃.

IWGO-WeP-34 Investigation of Temperature-Dependent Forward Transport Mechanism in kV class NiO/ β -Ga₂O₃ Heterojunction Diodes, Surajit Chakraborty, Deb Indronil Sajib, Uttam Singiseti, University at Buffalo-SUNY

Combining the ultra-wide bandgaps of p-NiO and n- β -Ga₂O₃ enables heterojunction diodes to achieve breakdown voltages exceeding 8 kV and power figures of merit (13.2 GW/cm²) [1]. In this study, we investigate the forward current behavior of sputtered p-NiO_x/n- β -Ga₂O₃ vertical rectifiers using temperature-dependent current–voltage (*I*–*V*–*T*) analysis, together with our developed analytical model and TCAD simulation incorporating Danielsson trap assisted interface recombination model [2].

We fabricated p-NiO_x/n- β -Ga₂O₃ HJD using RF reactive sputtering of a metallic Ni target for the NiO_x layer. The device schematic is illustrated in Fig. 1(a), with the process flow shown in Fig. 1(b). A bilayer NiO_x deposited with controlled Ar/O₂ ratios: the first layer is deposited at Ar/O₂ = 22/10 sccm (4.5 mT, 200 W, 100 nm), followed by a second layer at Ar/O₂ = 10/8 sccm (4 mT, 150 W, 100 nm), yielding sheet resistances of 171 k Ω /sq and 57.1 k Ω /sq, respectively. The doping concentration (*N_D*–*N_A*), extracted from C–V measurements, is $\sim 9 \times 10^{15}$ cm⁻³ which is depicted in Fig. 2. A small-area HJD (75 μ m diameter) with *V_{on}* \sim 1.97 V, an on-resistance of 16.3 m Ω /cm² achieves a breakdown voltage exceeding 3 kV (Instrument limit) showed in Fig. 3 and Fig. 4 respectively.

Temperature-dependent *I*–*V* measurements were conducted over a range from –33 °C to 250 °C to elucidate the forward conduction mechanism. To understand the mechanism, we developed both an analytical and TCAD model with interface recombination as the mechanism for current transport. This trend is in close agreement with the TCAD simulation model, as illustrated in Fig. 5. For all temperatures, *k_BT* \ll ΔE_c + *V_{bi}*, ruling out thermionic emission as the dominant transport mechanism. Furthermore, since *V_{ON}* \ll ΔE_c + *V_{bi}*, diffusion-limited transport is also unlikely. Silvaco TCAD simulations incorporating an interface trap level of approximately 0.4 eV below the NiO-side electrostatic potential successfully reproduce the *J*–*V* characteristics, showing close agreement with the experimental results depicted in Fig. 6 in different temperatures. Both the analytical and TCAD models predict the lower turn-on voltages than the voltage estimated from thermionic transport shown in Fig. 7. These results indicate that forward conduction is governed primarily by trap-assisted interface recombination.

IWGO-WeP-35 Group-III Flux Etching of β -(Al_xGa_{1-x})₂O₃ Heterostructures, Emma Rocco, Frank Kelly, J. S. Lundh, Daniel Pennachio, Katie Gann, Cameron Gorsak, Alan Jacobs, Marko Tadjer, Michael Mastro, U.S. Naval Research Laboratory

Group-III (Al, Ga) oxides have emerged as next-generation semiconductor materials for high-power applications owing to large bandgap energies and high critical electric field strengths. Realizing β -(Al_xGa_{1-x})₂O₃ power electronic devices require processing techniques for the fabrication of device architectures such as diodes and field effect transistors (FETs), including etching processes. Industry standard dry processes including inductively coupled plasma (ICP) etching have been developed for β -Ga₂O₃, utilizing SF₆, Cl₂, and BCl₃ chemistries. However, dry etching of β -Ga₂O₃ has been shown to result in subsurface damage. An alternative, Ga-flux etching of β -Ga₂O₃ has emerged as a potential damage-free technique and can be completed *in situ* via molecular beam epitaxy (MBE) and metal organic chemical vapor deposition (MOCVD). Ga-flux etch rates of β -Ga₂O₃ have been shown to vary based on the rate of Ga-flux, pressure, and crystal orientation, with etch rates as high as 140 nm/min and 30 nm/min reported for MOCVD and MBE flux etching, respectively. Etch rate has also been found to be dependent on feature size and pitch, with significant increase at the edge of mask openings due to precursor loading. To date, Ga-flux etching of β -(Al_xGa_{1-x})₂O₃ has yet to be reported, as well as the use of a combined Ga- and Al-flux.

In the present study, we investigate the impact of Ga to Al ratio, and group-III flux on the etch rate of β -(Al_xGa_{1-x})₂O₃ and Ga₂O₃ thin films. The structures under test are FETs consisting of O₃-MBE grown 21 nm β -(Al_{0.18}Ga_{0.82})₂O₃/250 nm Ga₂O₃ on (010) Ga₂O₃:Sn substrates (NCT, Japan). An SiO₂/SiN bi-layer mask is utilized and openings to the β -(Al_xGa_{1-x})₂O₃ are patterned via photolithography. Group-III flux etches were carried out in an Agnition Agilis 500 MOCVD system utilizing triethylgallium (TEGa) and trimethylaluminum (TMAI) as the Ga and Al precursors, respectively. A 24 min, Ga-flux only etch with TEGa flow rate of 35 μ mol/min resulted in etch

depths on the order of hundreds of nanometers, as measured by profilometry with an inverse relationship between etch depth and feature spacing. Characteristic crystallographic striations are seen via optical microscopy on the Ga₂O₃ surface following the etch for features with 5 μ m spacing. At increased feature spacings of 10 μ m and 15 μ m, incomplete removal of the Al-containing layer is observed by scanning electron microscopy and electron dispersive x-ray spectroscopy (SEM- EDX). This may indicate the formation of an Al or Al₂O₃ layer, inert to Ga-flux etching, resulting in micro-masking. Lower Ga- and group-III fluxes will be investigated for uniform volatilization of (Al_xGa_{1-x})₂O₃.

IWGO-WeP-36 Carrier Transport Across Wafer Bonded (001) -Ga₂O₃ Interfaces, Advait Gilankar, Arizona State University; Michael Liao, Piyush Shah, Apex Microdevices; Mark Goorsky, University of California Los Angeles; Nidhin Kurian Kalarickal, Arizona State University

Wafer bonding and heterogenous integration of β -Ga₂O₃ have been explored in the past to mitigate the low thermal conductivity of Ga₂O₃ [1]. However, homogeneous wafer bonding of Ga₂O₃ to Ga₂O₃ for active electrical transport across the bonded interface hasn't been explored so far. Achieving linear electrical transport across such homogeneously bonded interfaces with low interfacial resistance can open new design avenues for Ga₂O₃ power devices. In this work, we investigate electrical transport across bonded (001) Ga₂O₃ HVPE grown epilayers. Both samples underwent standard RCA SC-1 cleaning prior to being subjected to a plasma surface treatment. After plasma treatment, both samples were aligned face-to-face and \sim kPa pressure was applied to initiate the bond at room temperature. The bonded structure was then annealed up to 900 °C for bond strengthening. The topside epilayer (EPI2) and substrate were then polished at an angle to obtain an inclined surface (Fig.1 a). After polishing, EPI2 exhibited an RMS surface roughness of \sim 0.25 nm. Off-axis XRD ϕ -scans revealed an in-plane rotational misalignment of \sim 5° between the two bonded epilayers. The electrical transport across interface was studied by fabricating Ni/Ga₂O₃ SBDs and Si implanted ohmic contacts (Ti/Au) at different locations along the incline (Fig.1 a). Diodes formed directly of EPI1 displayed high current density (\sim 10² A/cm²), while diodes located just near the start of the incline (diode B) displayed no current. As we move to the location of diode C (thicker EPI2), the devices turn-on with a low forward current density (\sim 10⁻¹ A-cm⁻²) indicating high interfacial resistance. The diodes formed on the substrate (diode D) show high reverse leakage but similar forward current densities (\sim 10⁻¹ A-cm⁻²). We attribute this behavior to a fixed negative charge at the bonded interface (\sim high 10¹¹ cm⁻²), supported by Silvaco TCAD simulations, which showed clear current suppression with increasing interfacial fixed negative charge density. Similar to the diodes, Si-implanted and annealed ohmic contacts (along the incline of EPI2) exhibited quasi-ohmic behavior with high resistance. We hypothesize that reducing the rotational misalignment can result in enhanced current transport across the homogenous bonded interface. This work was supported by the National Science Foundation under Grant No. NSF ECCS 2336397.

[1] M. Liao, *J. Vac. Sci. Technol. A* 41, 063203 (2023).

*Author for correspondence: agilanka@asu.edu

IWGO-WeP-37 High-Reflectance In-Plane Ga₂O₃/Air DBRs Fabricated by HEATE on (010) β -Ga₂O₃, SOTARO IJIMA, TAKAHASHI YUKI, Sophia Univ, Japan; AKIHIKO KIKUCHI, Sophia Univ / Sophia Semiconductor Research Institute, Japan

Ga₂O₃ has attracted increasing interest for electronic and photonic devices, owing to its wide bandgap energy (> 4.5 eV), excellent controllability of n-type conductivity, and availability of high-quality single-crystal substrates. We have previously developed a hydrogen environment anisotropic thermal etching (HEATE) technique enabling precise, high-aspect-ratio nanofabrication of GaN and Ga₂O₃ via hydrogen-assisted thermal decomposition combined with an ultrathin SiO₂ mask.

In this study, we demonstrate a novel photonic device application based on (010) β -Ga₂O₃. An in-plane high-Q resonator was fabricated by integrating a Ga₂O₃/air distributed Bragg reflector (DBR), designed for broadband high reflectance in the visible region, with a nanofluidic channel for dye injection. The reflectance characteristics of standalone Ga₂O₃/air DBR structures were also investigated.

The integrated resonator consists of a dye-solution reservoir (300 μ m \times 500 μ m), a nanofluidic channel transporting dye via capillary action, and a resonator section with DBRs on both sides of the channel. To secure optical paths for side excitation and observation of resonator characteristics, high-aspect-ratio structures with heights exceeding 10 μ m were formed approximately 50 μ m from the substrate edge.

Wednesday Evening, August 5, 2026

Fabrication was carried out on Fe-doped (010) β -Ga₂O₃ wafers. After forming SiO₂ nanomasks by electron-beam lithography and dry etching, HEATE processing was performed at 900°C under a hydrogen pressure of 100Pa for 330min. High-resolution SEM revealed vertically smooth DBR sidewalls along the thermodynamically stable (100) planes. The Ga₂O₃/air layer thicknesses were 217nm/410nm for the third-order DBR and 362nm/683nm for the fifth-order DBR, with deviations from the designed values within +4nm and -10nm. Side-view optical microscope observations using a 100× objective lens clearly resolved the 16μm-high DBR structures and nanofluidic channels, confirming suitability for side-excited resonator characterization.

For optical characterization, the third- and fifth-order standalone DBRs, both designed for a center wavelength of 547nm, were fabricated. Reflectance spectra measured using Fourier imaging microscopy agreed well with one-dimensional transfer-matrix simulations. Maximum reflectance and stopband widths (reflectance >90%) were 97% and 62nm for the third-order DBR, and 95% and 35nm for the fifth-order DBR, demonstrating excellent broadband reflectance performance.

Acknowledgement: Part of this study was supported by JSPS KAKENHI JP24K00950.

References: [1] R. Kita et al., Jpn. J. Appl. Phys., 54, 046501 (2015). [2] Y. Ooe et al., 80th JSAP Autumn meeting, 21p-B31-6 (2019).

IWGO-WeP-38 Phase-Dependent Photoluminescence of Near-Infrared Color Centers in Ga₂O₃, Keidai Toyoshima, The University of Tokyo, Japan; *Mathias Marchal*, Technical University of Denmark, Denmark; *Riena Jinno*, Satoshi Iwamoto, The University of Tokyo, Japan

Color centers are localized electronic states associated with point defects in crystals, and light emission from these defects produces photons at wavelengths corresponding to these levels and has attracted interest for quantum applications. Recently, luminescence originating from color centers has been reported in beta gallium oxide (β -Ga₂O₃). One example is the emission at 1316 nm, which lies in the telecom O-band. This emission is thought to originate from transition-metal-related defects; although Cu³⁺-related complex defects are candidates, their exact origin remains unknown. Furthermore, the Debye-Waller factor, which quantifies the fraction of emission into the zero-phonon line relative to the total emission and serves as an important figure of merit for quantum applications, has not yet been evaluated for these color centers, nor have their formations in different crystal polymorphs been systematically investigated. In this study, we determine the Debye-Waller factor and investigate the photoluminescence (PL) of various Ga₂O₃ samples.

The samples include Fe-doped and unintentionally doped (UID) β -Ga₂O₃ (010) substrates, as well as Sn-, Cu-, and Fe-doped and UID α -Ga₂O₃ thin films grown on c-plane sapphire substrates. α -Ga₂O₃ thin films were grown by mist chemical vapor deposition (mist CVD). The dopants were added at a concentration of 0.01 at.% relative to Ga. The film thickness was ~800 nm. PL was measured at 9 K using a liquid helium cryogenic system with pulsed laser excitation at a wavelength of 700 nm.

Sharp emission lines around 1312.5 and 1316 nm were observed in the Fe-doped and UID β -Ga₂O₃ substrates. The Debye-Waller factor of the emission from the β -Ga₂O₃ substrates was estimated to be ~6% for both samples. In contrast, no corresponding peaks were detected in the α -Ga₂O₃ thin films. A peak observed at ~1150 nm in the α -Ga₂O₃ films was also observed when only the sapphire substrate was measured, suggesting it originated from color centers within the substrate.

The observation of telecom-band emission in UID β -Ga₂O₃ suggests that unintended defect formation readily occurs, making precise defect control in the β -phase challenging. In contrast, the absence of such emissions in α -Ga₂O₃, even when intentionally doped with transition metals, suggests that the formation of these color centers depends on the specific crystal structure of the β -phase. The absence of such unintended emissions makes α -Ga₂O₃ as a relatively clean and promising host material. By elucidating the precise phase-dependent mechanism of these defects, future studies could enable the controlled introduction and precise tuning of quantum emitters within α -Ga₂O₃ matrices.

IWGO-WeP-39 Transmutation-doped β -Ga₂O₃ via Thermal Neutron Irradiation, Richard Barber, University of Missouri; *Marko Tadjer*, Evan Glaser, Naval Research Laboratory; *Marc Weber*, Washington State University; *Alison Hartman*, University of Missouri-Columbia; *Jaime Freitas*, *Steven Bennett*, *Mason Klemm*, *Alan Jacobs*, *Karl Hobart*, Naval Research Laboratory; *Kohei Sasaki*, *Akito Kuramata*, Novel Crystal Technology, Japan; *P. Shiv Halasyamani*, University of Houston; *Blaine Reid*, *John Brockman*, *John Gahl*, University of Missouri

Technology for doping control of β -Ga₂O₃ crystals via thermal neutron transmutation doping (NTD) is proposed for producing controllably Ge-doped ($\sim 10^{15}$ - 10^{17} cm⁻³ Ge donor concentration) β -Ga₂O₃ wafers for high-voltage applications. Thermal neutron capture by the stable isotopes of Ga, ⁶⁹Ga and ⁷¹Ga, produce the unstable isotopes ⁷⁰Ga and ⁷²Ga, which decay into stable ⁷⁰Ge and ⁷²Ge, forming shallow (*E*_c-28 meV) donors in Ga₂O₃.

NTD of Ga₂O₃ has been proposed by Logan et al. and demonstrated by Irvine et al. who have shown the transmutation of ^{69/71}Ga into stable ^{70/72}Ge via thermal neutron capture and decay at the OPAL research reactor in Australia [1, 2]. While successfully producing ^{70/72}Ge in β -Ga₂O₃, their work experienced significant challenges originating from the Ir impurities in the Ga₂O₃ wafers and the compensating point defects generated by fast neutrons. In our experiments, β -Ga₂O₃ wafer purity was significantly improved via growth in a crucible-free float zone (FZ) reactor. FZ crystals with diameter of about 8-10 mm were grown and subsequently prepared into polished (010) β -Ga₂O₃ wafers at Novel Crystal Technology, Japan.

In our presentation we will discuss the thermal neutron doping that we performed on Ga₂O₃ FZ grown samples. Point defect formation caused by the fast neutron component of the flux was characterized via electron paramagnetic resonance (EPR) spectroscopy and positron annihilation spectroscopy (PAS), demonstrating suppression of Ga-related vacancies under the irradiation and annealing conditions in these experiments. As a result, for 5×10¹³ n/s·cm² flux duration for 20 hrs, a 4.17×10¹⁷ cm⁻³ (0.511 ng/mol) concentration of ^{70/72}Ge was measured via inductively-coupled plasma mass spectroscopy (ICP-MS) and confirmed by electron paramagnetic resonance (EPR).

In these samples, a gallium vacancy related point defect concentration of $\sim 9 \times 10^{15}$ cm⁻³ was measured via positron annihilation spectroscopy (PAS) and a pre-irradiation Si concentration of $\sim 3 \times 10^{16}$ cm⁻³ was measured via secondary ion mass spectroscopy (SIMS). To our knowledge, this result is the first experimental demonstration of a ^{70/72}Ge-doped β -Ga₂O₃ crystal with a net thermal neutron transmuted donor concentration higher than the net vacancy concentration induced by the fast neutron component of the irradiation flux.

[1] C.P. Irvine et al., Physical Review Materials 6, no. 11 (2022): 114603

[2] J.V. Logan et al., Mater. Adv. 1, no. 1 (2020): 45-53.

IWGO-WeP-40 Optimizing β -Ga₂O₃ MOCVD Regrowth for Vertically Scaled Channels, Julian Gervasi-Saga, *Nabasinhu Das*, *Advait Gilankar*, *Nidhin Kurian Kalarickal*, School of Electrical, Computer and Energy Engineering, Arizona State University

Vertically scaled channels (Si delta doping, β -Ga₂O₃/(AlGa)₂O₃ modulation doping) are essential for realizing RF and mm-wave transistors based on β -Ga₂O₃. Contact regrowth using both MBE and MOCVD has proven highly effective for forming ohmic contacts to β -Ga₂O₃. While very low contact resistivity ($\sim 10^{-7}$ Ω·cm²) has been demonstrated for metal-n⁺⁺ β -Ga₂O₃ contacts [1], the **total contact resistance** (metal-to-channel) typically remains greater than 1 Ω·mm, particularly in vertically scaled channel architectures. This is nearly an order of magnitude higher than values routinely achieved in GaN (~ 0.1 Ω·mm) and must be reduced to minimize RC delays in high-frequency transistors. In this work, we investigate the impact of the source/drain recess etch and in-plane anisotropy on the total contact resistance.

The total contact resistance (*R*_c^{total}) comprises the metal-n⁺⁺ contact resistance (*R*_cⁿ⁺⁺), the resistance between the metal and regrown layer (*R*_sⁿ⁺⁺), and the interfacial resistance (*R*_{int}) between the regrown layer and channel. A source/drain recess etch, typically performed via ICP-RIE, exposes the channel sidewall prior to regrowth but can introduce etch-induced damage, particularly at the sidewalls, degrading the interfacial resistance. To evaluate this, we compare ICP-RIE etches and an in-situ TBCL etch and assess their impact on contact resistance. The epilayers were co-loaded β -Ga₂O₃ (010) MOCVD-grown Si delta-doped samples (sheet charge $\sim 1 \times 10^{13}$ cm⁻²) with a 30 nm cap. Four etch processes were studied: low-power BCl₃ ICP, low-power Cl₂ ICP, high-power BCl₃ ICP, and in-situ TBCL etching prior to regrowth. After regrowth, Ti/Au contacts were deposited

and annealed at 470 °C in N₂. Electrical characterization was performed using TLM. The low-power BCl₃ ICP etch yielded the lowest contact resistance (**0.54 Ω-mm**), followed by high-power BCl₃ (**2.44 Ω-mm**), low-power Cl₂ (**7.16 Ω-mm**), and in-situ TBCl (**12.08 Ω-mm**). The etch process significantly affected the sheet resistance of the regrown n⁺ layer, indicating defect formation originating at the etched surface. Pronounced in-plane anisotropy in contact resistance was also observed, primarily attributed to variations in R_{int}. TLM structures along [001] exhibited the highest resistance, while those along [100] showed the lowest. Our work highlights the critical role of recess etch processes and in-plane anisotropy in determining contact resistance in β-Ga₂O₃ devices.

This work is supported by the Army Research Office UWBG RF Center (W911NF2520005) and the National Science Foundation (NSF ECCS 2336397).

[1] A. Bhattacharyya et al., Appl. Phys. Express 14, 076502 (2021).
Author for correspondence: jgervass@asu.edu

IWGO-WeP-41 962 V Ga₂O₃ Schottky Power Diodes on (011) Substrate, Luoyuan Jiang, Md Mosarof Hossain Sarkar, Yibo Xu, Hongping Zhao, Wu Lu, Ohio State University

Gallium oxide (Ga₂O₃) has attracted increasing attention for high-voltage power devices due to its ultra-wide bandgap and large critical electric field. In particular, (011)-oriented β-Ga₂O₃ is considered promising for device applications because of lower dislocation density [1]. In this work, we show a Schottky diode with a breakdown voltage of 962 V on a (011) Ga₂O₃ substrate with significantly thinner drift layer thickness than reported devices with similar breakdown voltages.

The device structure consists of a 5.5-μm-thick drift layer grown by MOCVD at a growth rate of 5.5 μm/hr [2] on a (011)-oriented Ga₂O₃ substrate. To achieve a high breakdown voltage, a deep trench filled with SiO₂ in combination with a field plate is used for electric-field mitigation. Numerical simulations show that the structure with optimized trench depth and field plate geometry has a breakdown voltage of 1.4 kV, 800 V higher than the control structure without field management.

C-V measurements show that the average net donor concentration is ~1 × 10¹⁶ cm⁻³. The fabricated device with Ni/Au Schottky contacts exhibited a turn-on voltage of 0.98 V at 1 A/cm², an ideality factor of 1.11, and a specific on-resistance of 6.06 mΩ·cm². Temperature-dependent forward I-V measurements yielded a Schottky barrier height of 1.19 eV and a Richardson constant of 42.2 A/cm²/K². The leakage current density is 8.09 × 10⁻⁹ A/cm² at 100 V reverse bias, and the breakdown voltage is 962 V at a current density of 1 A/cm². At this voltage, the electrical field peaks at the anode edge with a value of 3.6 MV/cm. To our knowledge, the device has the thinnest drift layer thickness in comparison with reported Ga₂O₃ Schottky power diodes with a similar breakdown voltage. The results demonstrated from this work are promising for further scaling up the blocking voltage by increasing the drift layer thickness.

[1] B. Chen *et al*, CrystEngComm, 25, 2404–2409 (2023).

[2] M. M. H. Sarkar *et al*, ACS Appl. Electron. Mater. 8, 3, 1380–1389 (2026).

*Author for correspondence: jiang.2694@osu.edu
[mailto:jiang.2694@osu.edu]; lu.173@osu.edu

IWGO-WeP-42 Identifying the Origin of Emissions and Anisotropic Properties of Different Crystallographic Orientation Sn-Doped β-Ga₂O₃ Substrates, Kishor Upadhyaya, King Abdullah University of Science and Technology, India; Andres Hurtado, King Abdullah University of Science and Technology, Colombia; Hadeel Alamoudi, Iman Roqan, King Abdullah University of Science and Technology, Saudi Arabia

Photoluminescence (PL) and PL excitation (PLE) studies are necessary to understand the orientation dependent transition mechanisms and excitation pathways in β-Ga₂O₃. In this work, we address this gap by exploring the effect of Sn doping on the anisotropic optical properties of state-of-the-art quality (100), (010), and (001)-oriented single crystal Sn-doped β-Ga₂O₃ grown by EFG method (Novel crystal technology, Inc.). The absorption spectra of these Sn-doped β-Ga₂O₃ samples exhibit different behavior for different orientations with (100) and (100) orientations exhibiting an overlap between shallow and deep states with band edge states while (010) reveals a distinct separation between the shallow and deeper states. Raman spectroscopy indicates that the Sn substitution at octahedral Ga sites results in anisotropic vibrational behaviour by significantly altering B_g⁽⁵⁾ and A_g⁽⁹⁾ vibrational modes while suppressing A_g⁽⁹⁾ mode in (010) orientation whereas B_g⁽⁵⁾ is negligible in other two

orientations. PL spectra of Sn-doped films exhibit a broadband emission in the 2.5 eV-4.1 eV range with no band edge emission that is redshifted compared to their UID counterparts. PL and PLE measurements indicate such broadband emission is originated from UV, Blue and green components, while the contribution of each component is different for different orientation. Temperature-dependent photoluminescence (PL) measurements reveal red shift for all three orientations with (010) exhibiting the largest red shift of ~70 meV. PLE measurements at each component reveal the transitions related to such broad band for different orientation Sn-doped β-Ga₂O₃, which governed by dopant-related recombination paths as well as associated intrinsic defects and agrees with the absorption spectra. PLE spectra for (010) reveal additional peaks at 3.8 eV and 4.15 eV, which are not exhibited in other two orientations. PL obtained for different excitation energies corresponding to the peaks observed in PLE (3.35 eV - 4.95eV) reveal luminescence band due to even sub-band gap excitation energy of 3.35 eV. Such excitation-dependent PL correlates very well with the observed PLE peaks confirming the orientation dependent transitions. This is the first observation of emission from β-Ga₂O₃ with sub-band gap excitation. Time-resolved PL analysis shows that (010) exhibits fastest decay time of τ=22ms while (100) has the slowest decay time of τ=135ms further confirming the optical anisotropy. This study reveals origin of Sn-doped β-Ga₂O₃ broad emission, the related anisotropic properties and the effect of Sn incorporation in different orientation on the carrier recombination pathways.

Bold page numbers indicate presenter

- A —
 Alamoudi, Hadeel: IWGO-WeP-42, 11
 Alem, Nasim: IWGO-WeP-13, 3
 Alema, Fikadu: IWGO-WeP-15, 4
 Amir, Walid: IWGO-WeP-29, 7
 Anandan, Sai Kkrishna: IWGO-WeP-24, 6
 — B —
 Balog, Andrew: IWGO-WeP-13, 3
 Banner, Nathan S.: IWGO-WeP-33, 8
 Barber, Richard: IWGO-WeP-39, 10
 Beakes, Connor: IWGO-WeP-13, 3; IWGO-WeP-18, 4
 Bennett, Steven: IWGO-WeP-39, 10
 Berini, Bruno: IWGO-WeP-3, 1
 Bibilashvili, Amiran: IWGO-WeP-3, 1
 Brand, Will: IWGO-WeP-15, 4
 Brillson, Leonard: IWGO-WeP-16, 4
 Brockman, John: IWGO-WeP-39, 10
 Buontempo, Joshua: IWGO-WeP-10, 2
 Butenko, Pavel: IWGO-WeP-5, 1
 — C —
 Cantin, Jean-Louis: IWGO-WeP-3, 1
 Cavaleiro, Randal: IWGO-WeP-18, 4
 Chabak, Kelson: IWGO-WeP-4, 1
 Chakraborty, Surajit: IWGO-WeP-29, 7; IWGO-WeP-34, 9
 Chikoidze, Ekaterine: IWGO-WeP-3, 1
 Chiu, Chan-Wen: IWGO-WeP-33, 8
 Chujo, Taiki: IWGO-WeP-6, 2
 Crnobrnja, Aleksa: IWGO-WeP-11, 3
 — D —
 Das, Nabasindhu: IWGO-WeP-40, 10
 DeLeon, Carlos: IWGO-WeP-16, 4
 Dhora, Andri: IWGO-WeP-31, 8
 Dumont, Yves: IWGO-WeP-3, 1
 Dutton, Benjamin: IWGO-WeP-12, 3; IWGO-WeP-13, 3; IWGO-WeP-18, 4
 — F —
 Freitas, Jaime: IWGO-WeP-39, 10
 — G —
 Gahl, John: IWGO-WeP-39, 10
 Galyukov, Alex: IWGO-WeP-11, 3
 Gann, Katie: IWGO-WeP-26, 6; IWGO-WeP-28, 7; IWGO-WeP-30, 8; IWGO-WeP-35, 9
 Geddis, Kale: IWGO-WeP-12, 3
 Gervassi-Saga, Julian: IWGO-WeP-40, 10
 Gilankar, Advait: IWGO-WeP-36, 9; IWGO-WeP-40, 10
 Glaser, Evan: IWGO-WeP-39, 10
 Goorsky, Mark: IWGO-WeP-36, 9
 Gopalan, Sanjay: IWGO-WeP-17, 4
 Gorsak, Cameron: IWGO-WeP-10, 2; IWGO-WeP-28, 7; IWGO-WeP-30, 8; IWGO-WeP-35, 9
 Gray, Tia: IWGO-WeP-9, 2
 Green, Andrew: IWGO-WeP-4, 1
 — H —
 Hajzus, Jenifer: IWGO-WeP-28, 7
 Halasyamani, P. Shiv: IWGO-WeP-39, 10
 Hartman, Alison: IWGO-WeP-39, 10
 Hasegawa, Sho: IWGO-WeP-6, 2
 Haven, Drew: IWGO-WeP-12, 3; IWGO-WeP-13, 3; IWGO-WeP-18, 4
 Hickman, Austin: IWGO-WeP-15, 4
 Hobart, Karl: IWGO-WeP-30, 8; IWGO-WeP-39, 10
 Hurtado, Andres: IWGO-WeP-42, 11
 — I —
 Igarashi, Takuya: IWGO-WeP-6, 2
 IJIMA, SOTARO: IWGO-WeP-37, 9
 Imanishi, Masayuki: IWGO-WeP-20, 5; IWGO-WeP-21, 5
 Ishikawa, Masato: IWGO-WeP-7, 2
 Ishizawa, Satoshi: IWGO-WeP-22, 5
 Iwamoto, Satoshi: IWGO-WeP-38, 10
 — J —
 Jacobs, Alan: IWGO-WeP-27, 7; IWGO-WeP-28, 7; IWGO-WeP-30, 8; IWGO-WeP-35, 9; IWGO-WeP-39, 10
 Jiang, Luoyuan: IWGO-WeP-41, 11
 Jinno, Riena: IWGO-WeP-38, 10
 Joyce, David: IWGO-WeP-12, 3; IWGO-WeP-13, 3; IWGO-WeP-18, 4
 Jung, Yusup: IWGO-WeP-1, 1
 — K —
 Kalarickal, Nidhin Kurian: IWGO-WeP-36, 9; IWGO-WeP-40, 10
 Kamada, Kei: IWGO-WeP-22, 5
 Kanegae, Kazutaka: IWGO-WeP-2, 1
 Kang, Jinki: IWGO-WeP-8, 2
 Kang, Myeonggyun: IWGO-WeP-22, 5
 Kang, TaiYoung: IWGO-WeP-1, 1
 Kao, Ming-Chao: IWGO-WeP-25, 6
 Kelemen, Paul: IWGO-WeP-33, 8
 Kelly, Frank: IWGO-WeP-26, 6; IWGO-WeP-27, 7; IWGO-WeP-28, 7; IWGO-WeP-30, 8; IWGO-WeP-35, 9; IWGO-WeP-9, 2
 KIKUCHI, AKIHIKO: IWGO-WeP-37, 9
 Kim, Ki Wook: IWGO-WeP-17, 4
 Kim, Min-Yeong: IWGO-WeP-24, 6; IWGO-WeP-4, 1
 Kim, Sanghun: IWGO-WeP-1, 1
 Kioupakis, Emmanouil: IWGO-WeP-14, 3
 Kitahara, Masanori: IWGO-WeP-22, 5
 Klemm, Mason: IWGO-WeP-39, 10
 Koo, Sang-Mo: IWGO-WeP-4, 1
 Koshi, Kimiyoshi: IWGO-WeP-6, 2
 Krishnamoorthy, Sriram: IWGO-WeP-32, 8; IWGO-WeP-9, 2
 Kuball, Martin: IWGO-WeP-24, 6
 Kuramata, Akito: IWGO-WeP-39, 10; IWGO-WeP-6, 2
 Kushitashvili, Zurab: IWGO-WeP-3, 1
 Kyoung, SinSu: IWGO-WeP-1, 1
 — L —
 Lavelle, Robert: IWGO-WeP-12, 3; IWGO-WeP-13, 3; IWGO-WeP-18, 4
 Lee, Dong-Jun: IWGO-WeP-8, 2
 Lee, Sohyun: IWGO-WeP-33, 8
 Li, Qiliang: IWGO-WeP-4, 1
 Liao, Michael: IWGO-WeP-36, 9
 Liddy, Kyle: IWGO-WeP-4, 1
 Lindquist, Kurt: IWGO-WeP-12, 3
 Liu, Jiawei: IWGO-WeP-29, 7
 Liu, Yizheng: IWGO-WeP-9, 2
 Lu, Wu: IWGO-WeP-41, 11
 Lundh, J. S.: IWGO-WeP-35, 9
 Lundh, James: IWGO-WeP-27, 7
 Lyle, Luke: IWGO-WeP-12, 3; IWGO-WeP-13, 3; IWGO-WeP-18, 4
 Lyle, Luke A. M.: IWGO-WeP-33, 8
 — M —
 Maimon, Ory: IWGO-WeP-4, 1
 Marchal, Mathias: IWGO-WeP-38, 10
 Masten, Hannah: IWGO-WeP-9, 2
 Mastro, Michael: IWGO-WeP-26, 6; IWGO-WeP-27, 7; IWGO-WeP-28, 7; IWGO-WeP-30, 8; IWGO-WeP-35, 9
 Mattapalli, Akhila: IWGO-WeP-32, 8
 Medjdoub, Farid: IWGO-WeP-3, 1
 Micottis, Tom: IWGO-WeP-3, 1
 Mohney, Suzanne E.: IWGO-WeP-33, 8
 Mori, Yusuke: IWGO-WeP-20, 5; IWGO-WeP-21, 5
 Moser, Neil: IWGO-WeP-4, 1
 Mouck, Donivan R.: IWGO-WeP-33, 8
 Murakami, Rikito: IWGO-WeP-22, 5
 Muth, John: IWGO-WeP-17, 4
 Myers-Ward, Rachael: IWGO-WeP-30, 8
 — N —
 Nair, Hari: IWGO-WeP-10, 2
 Nakano, Haru: IWGO-WeP-20, 5
 Nandi, Arpit: IWGO-WeP-24, 6
 Nath Saha, Chinmoy: IWGO-WeP-32, 8; IWGO-WeP-9, 2
 Nelson, Tolen: IWGO-WeP-27, 7
 Nishinaka, Hiroyuki: IWGO-WeP-2, 1
 — O —
 Osinsky, Andrei: IWGO-WeP-15, 4
 — P —
 Park, Taejun: IWGO-WeP-1, 1
 Patel, Satyam: IWGO-WeP-19, 5
 Patnaik, Akash: IWGO-WeP-3, 1
 Pennachio, Daniel: IWGO-WeP-26, 6; IWGO-WeP-27, 7; IWGO-WeP-28, 7; IWGO-WeP-35, 9
 Peterson, Becky (R.L.): IWGO-WeP-19, 5
 Peterson, Carl: IWGO-WeP-32, 8
 Pistner, Scott: IWGO-WeP-13, 3; IWGO-WeP-18, 4
 Pookpanratana, Sujitra: IWGO-WeP-4, 1
 — R —
 Rebollo, Steve: IWGO-WeP-32, 8
 Redwing, Joan: IWGO-WeP-13, 3
 Reid, Blaine: IWGO-WeP-39, 10
 Ribault, Thomas: IWGO-WeP-3, 1
 Rocco, Emma: IWGO-WeP-26, 6; IWGO-WeP-27, 7; IWGO-WeP-28, 7; IWGO-WeP-30, 8; IWGO-WeP-35, 9
 Roqan, Iman: IWGO-WeP-42, 11
 — S —
 Sajib, Deb Indronil: IWGO-WeP-34, 9
 Sakaguchi, Ryoichi: IWGO-WeP-6, 2
 Sarkar, Md Mosarof Hossain: IWGO-WeP-41, 11
 Sartel, Corinne: IWGO-WeP-3, 1
 Sasaki, Kohei: IWGO-WeP-39, 10; IWGO-WeP-6, 2
 Shah, Piyush: IWGO-WeP-36, 9
 Shimazaki, Takumi: IWGO-WeP-7, 2
 Shinagawa, Ryo: IWGO-WeP-6, 2
 Shrestha, Pragya: IWGO-WeP-4, 1
 Singiseti, Uttam: IWGO-WeP-29, 7; IWGO-WeP-34, 9
 Smirnov, Andrey: IWGO-WeP-11, 3
 Snyder, David: IWGO-WeP-13, 3; IWGO-WeP-18, 4
 Speck, Jim: IWGO-WeP-32, 8
 Suezumi, Hisato: IWGO-WeP-22, 5
 — T —
 Tadjer, Marko: IWGO-WeP-27, 7; IWGO-WeP-30, 8; IWGO-WeP-35, 9; IWGO-WeP-39, 10; IWGO-WeP-9, 2
 Tanikawa, Hayato: IWGO-WeP-2, 1
 Togashi, Rie: IWGO-WeP-7, 2
 Toyoshima, Keidai: IWGO-WeP-38, 10
 Tripathi, Pushpanshu: IWGO-WeP-10, 2
 — U —
 Ueda, Yuki: IWGO-WeP-6, 2
 Upadhyaya, Kishor: IWGO-WeP-42, 11
 Usami, Shigeyoshi: IWGO-WeP-20, 5; IWGO-WeP-21, 5
 — W —
 Weber, Marc: IWGO-WeP-39, 10
 Welp, Eric: IWGO-WeP-13, 3
 — X —
 Xu, Yibo: IWGO-WeP-41, 11
 — Y —
 Yokota, Yuui: IWGO-WeP-22, 5
 Yoshikawa, Akira: IWGO-WeP-22, 5
 Yoshino, Masao: IWGO-WeP-22, 5
 YUKI, TAKAHASHI: IWGO-WeP-37, 9

Author Index

— Z —

Zhang, Haizhong: IWGO-WeP-23, **6**
Zhang, Kaitian: IWGO-WeP-16, 4

Zhang, Xiao: IWGO-WeP-14, **3**
Zhao, Hongping: IWGO-WeP-16, 4; IWGO-
WeP-41, 11

Zheng, Yunlin: IWGO-WeP-3, 1